(12)

SPECIAL TECHNICAL REPORT

AD-A169 474

ARPA Order No.: 9031 Program Code No.: 5221

Contractor: Boeing Aerospace Company (A Division of The Boeing Company)

Contract No.: N00014-85-C-0039 Contract Amount: $10,155,862

Effective Date of Contract: 12 November 1984

Expiration Date of Contract: 31 October 1986

Program Manager: Donald R. Shoffstall

Telephone No.: (206)655-8220

Principal Investigator: John L. Adamski

Telephone No.: (206)655-2605

Short Title of Work: Visible FEL

Title of Special Technical Report: FEL Optics Coating Test Program (Design Phase of Sample Introduction Chamber), Deacon Research, February 1986

RE: Processing of Two Related Documents
These two reports should be processed as one report.
Per Mrs. Catherine McKelleget, ONR/Code 1112

Deacon Research
900 Welch Road
Suite 203
Palo Alto CA 94304

Final Report
to
Boeing Aerospace Corporation

FEL OPTICS COATING TEST PROGRAM

(Design phase of sample introduction chamber)

Principal Investigator: David A. G. Deacon
Research Physicist
(415) 326-1520

Abstract

We have completed the design of an experiment which will allow us to determine the nature and the rates of the UV degradation process in free electron laser mirror coatings. We summarize the main information requirements of the FEL community, and describe the system design which is driven by these requirements. We are prepared to begin construction of the basic system as soon as funding is allocated; the design of the carbonaceous gas chamber should proceed in the interim.

February 1986

Table of Contents

1. Program Goals

The performance of the free electron laser for the directed energy weapons application depends critically on only three technologies: the high brightness accelerator, the FEL amplifier, and the cavity optics. Our goal in this program is to examine the performance of the optical elements under the combined loading of the fundamental and the harmonic emissions of the FEL amplifier.

The performance of both the RF linac based FEL and the induction linac based FEL may be subject to significant limitations due to UV-induced absorption in the early optical elements following the FEL amplifier. These limitations are expected to appear suddenly at a certain fluence level, with little warning. Our central objective in this program is to measure the rate of the UV induced absorption, and to identify the scaling parameters so that we can predict with some confidence the performance limitations of the optics. When these limits are reached in the experimental programs, a knowledge of the scaling relations and possible countermeasures will be invaluable in planning an appropriate response to the problem.

2. Description of the Principal Test Requirements

a) Experimental Requirements

The equipment required for UV damage testing follows primarily from the signal requirements. An intense source of radiation must be used with a sufficiently sensitive absorption measurement tool in a well characterized vacuum environment.

Under the low vacuum conditions of the Orsay storage ring ACO, a fluence in the range of 10^{15} to 10^{17} photons/cm^2 is required to produce the initial bulk absorption which appears to saturate at around 10^{-3} absorption. We do not yet know the exact fluence required to provoke and saturate this effect. During the early measurements, the undulator could not be switched on or off fast enough to identify the rates for this process. The shutter which has now been installed in the Orsay system makes it possible to produce a short controlled exposure. Multiple measurements of the bulk effect prior to saturation will yield us the rate of absorption increase.

The part of the damage process which is produced at the surface of the optic requires higher fluence levels, but has no well defined saturation. In the original experiments, about 10^{19} photons/cm^2 were required to produce 10^{-3} absorption. It is clear that to study the scaling of these processes, a UV source is required which can supply a fluence on the order of 10^{20} /cm^2 in a reasonable time. Only the storage ring mounted undulator and

the tapered wiggler FEL itself produce enough UV to satisfy these criteria. It is preferable to use the storage ring based source for the optics characterization effort since the undulator sources are available now, and require no additional effort to keep them operating. Since the operation of the undulator is independent of the performance of the mirrors, a very important degree of flexibility is available with the storage ring based UV source.

Among the undulator sources now in operation or close to it, only NOEL at Orsay and WUNDER at Stanford operate in the near UV range where the damage occurs. NOEL is the preferred source since it is fully operational, well characterized, and it covers the full photon energy range from 1 eV to 100 eV.

Any source of undulator radiation operates in vacuum, but the intense storage ring sources must operate at or below 10^{-10} Torr in order to maintain the lifetime of the stored beam. Foreign contaminants in the atmosphere, particularly carbon and those of high Z, are rigorously excluded. Any system which communicates directly with the storage ring environment (which means all UV experiments) must take the appropriate measures to exclude such contaminants from flowing into the storage ring vacuum chamber.

This experiment requires interchange of optics into and out of the UV beam produced by NOEL. A sample introduction chamber is required for this purpose, which can be sealed off from the ring

vacuum securely. Optics to be exposed can be placed into the sample introduction chamber at atmospheric pressure; the chamber must be pumped down to a lower pressure than the ring vacuum before the storage ring lab will allow the communicating valve to be opened. The pumpdown time is on the order of 24 hours even with large pumps, so provisions must be made to store many samples in the introduction chamber if a significant number of measurements are to be made. If in addition controlled amounts of carbonaceous gasses are to be released in the vicinity of the sample under exposure, provision must be made for differential pumping between the sample and the main ring vacuum. This chamber should be independent from the sample introduction chamber to allow the early experiments to proceed while the differentially pumped chamber is being fabricated and leak checked.

The final experimental requirement is for an absorption measurement system capable of measuring the small changes induced in the mirrors after a short exposure time of, say, a minute. To obtain this information with a signal to noise ratio of ten to one implies that the noise level must be at or below 1 ppm. The only instrument capable of providing this level of performance is the ringdown cavity lossmeter. Fortunately, this device is now available commercially (through Deacon Research) so no time needs to be allocated to develop this technology by the project. With minor modification to the beam transport and mode matching schemes, a resolution of 1 ppm is available throughout the visible region of the spectrum. Good performance is also available in the near UV and the IR spectral regions which can be

reached by doubling or Raman shifting the tunable dye laser source.

b) Test Objectives

The objectives of this program are to identify the scaling relations of the UV damage and to measure the rate constants for the effect on the Boeing "burst mode" oscillator mirrors. Deacon (Appendix A) has recently published an analysis of the Orsay results which postulates that carbon is progressively integrated into the surface structure when UV light is present. This mechanism has three unknown rate constants which describe the effects of the pressure, the sample temperature, and the UV intensity on the damage rate. These constants can be determined if the pressure, intensity, and temperature of the sample can be varied in the test chamber. They can be expected to have some dependence on the optical material being exposed, the UV photon energy, and the net fluence. In this program, it would be possible to ascertain the applicability of the model, and to measure the relevant rate constants in the parameter range available to the apparatus.

The list of questions to be answered on this problem is long. They are summarized in Table I and discussed below.

The initial question to be resolved is the scaling of the induced absorption as a function of fluence. No detailed

1. Measure the UV induced absorption as a function of fluence
   - is the fluence dependence cubic?
   - where does the absorption saturate?
   - are there multiple saturation fluences?
   - is there evidence of intensity dependence?

2. Measure the damage rate as a function of K, electron energy
   - which photon energy ranges do the damage?
   - are the damaging photons narrow-band?
   - is the photon energy dependent on the molecular species?
   - does the saturation depend on the UV photon energy?

3. Examine the rapid, saturating degradation phenomenon
   - how fast is the absorption growth?
   - how slow is the absorption decay in the dark?
   - can the absorption be bleached?
   - how does the saturated absorption depend on material?
   - how does it depend on the fabrication process?

4. Characterize the scaling with partial pressure
   - is the damage linear with pressure?
   - does the saturation level depend on pressure?
   - which gas species produce UV induced absorption?
   - what are the pressure vs. intensity scaling regimes?

5. Characterize the temperature dependence
   - how does the rate depend on sample temperature?
   - does the temperature influence the P-I dependence?
   - does temperature reduce the saturation levels?

6. Investigate countermeasures
   - does the presence of O_2 reduce the carbon growth rate?
   - are there other means of reducing the rate (cryopumping)?

7. Examine the materials dependence of the damage for
   - SiO_2/TiO_2
   - SiO_2/ZrO_2
   - SiO_2/HfO_2
   - SiO_2/Sc_2O_3
   - SiO_2/Ta_2O_5

8. Examine the dependence on fabrication technique for
   - neutralized ion beam deposition
   - e^- beam deposition
   - other techniques such as CVD, sol-gel

Table I: Issues to be resolved in the UV damage experiment.

measurements have ever been taken of the time dependence of the UV induced absorption. According to the surface cracking of carbon model, the damage rate should vary as the cube of the time at constant intensity. Bulk effects, on the other hand, are linear in the time. The simple measurement of absorption as a function of fluence can lend confirmation to or negate the proposed model (see Appendix). The interpretation of subsequent measurements also depends this result.

At high fluence levels, the induced absorption can be expected to saturate. The saturated absorption and the saturation fluence are critical quantities in the scaling to the FEL environment. Information may also be deriveable on the mechanism of the damage from the form of the structure in the absorption vs fluence curve.

Finally, it will be important to determine at this stage if any intensity dependence can be seen in the fluence curve. The carbon cracking model predicts that in one regime of operation, the degradation rate saturates at high intensities. The interpretation of all data acquired will depend on the operating regime. (The dependence on partial pressure of the various gasses and sample temperature is also important. However, in the initial configuration we will not have the capability to vary either of these quantities. A residual gas analyzer is required to determine that the partial pressures remain constant across time. No sharp dependence is expected on the temperature near 20 °C.)

Upon completion of these initial measurements, we can move on to the question of which harmonic is causing the damage. No harmonic filter exists in the Orsay beamline, so a sample would be exposed to all of the harmonics produced by the undulator. However, the relative strength of the harmonics of the undulator is adjustable by changing the magnetic field parameter K. It is therefore possible to determine the spectral region in which photons can produce absorption by measuring the rate of damage at several values of K. (The energy of the ring can be changed at the same time so that the harmonic frequencies remain constant.) If we know the dependence of the loss on fluence, the photon energy range can be determined from two or more measurements at different K parameters. Unfortunately, the result depends to some extent on the model which is assumed for the spectral dependence of the process. For this reason, it is also important to determine if the damaging photon energy band is broad or narrow. This can be done by measuring the rate as a function of energy for constant K, which scans the harmonic frequencies without changing their relative amplitude.

Once the differentially pumped vacuum chamber is in place and the partial pressures of the active gasses can be adjusted, it can also be determined if the active photon energy range depends significantly on the molecular species.

In a six month program, the first three issues in Table I can be addressed for a single set of samples. This much work should be done as a minimum characterization of the degradation.

The remainder of the issues can be investigated according to the available time.

The observation of rapid absorption increase on first exposure to the UV beam raises to prominence a second mechanism which is of concern to FEL designers. It is currently postulated that this process arises from the population of localized traps in the bandgap of the optical coating material. Since it saturates in the vicinity of 10^{-3} absorption and occurs rapidly, it will contribute an important part of the limiting absorption performance of FEL mirrors. By limiting the undulator dose on the mirrors at first exposure, we should be able to determine how fast the absorption grows as a function of fluence.

If the mechanism postulated above is correct, we will see an absorption growth rate slower than cubic in the time, but no slower than linear. To verify the postulated mechanism, we would also measure the decay time of the induced absorption and determine whether it can be bleached and whether the decay can be accelerated by heating the sample. If indeed the rate is proportional to the density of states in the band gap which are populated with electrons by the UV photons, the saturated absorption level would depend on the material and its fabrication process. At Orsay, it has already been observed that mirrors fabricated from SiO_2/Ta_2O_5 multilayers show twice the saturated absorption of SiO_2/TiO_2 mirrors made by the same process and by the same vendor. We would investigate the materials dependence over a wider class of materials discussed below, and examine the

difference between mirrors of identical materials but made by neutralized ion sputtering or e^- beam deposition.

Since one of the two major degradation processes involves the deposition of carbon at the surface of the optic, it is important to identify the scaling of the deposition as a function of the partial pressure of the various carbonaceous gasses typically found in the vacuum environment. These include mainly CO, CH_3OH, CO_2, CH_4, and C_2H_6, in about that order of importance for a well baked system. The rates should be measured to determine if the rate grows linearly with pressure, and if the slope is dependent on the intensity of illumination. A few gasses should be examined to determine if the deposition rate depends significantly on the species. The photon energy dependence of the deposition rate on the molecular species would also provide us with important information concerning the mechanism of the process.

Once the differentially pumped carbonaceous gas chamber is installed, some time should be dedicated to identify the scaling regimes of the induced absorption in the fully three dimensional pressure-intensity-temperature space. Elevating the temperature of the optical sample is now expected to reduce the degradation rate substantially. Measurements of the damage rate as a function of temperature could verify the functional form of the temperature dependence, and determine the exponential parameter and proportionality constant in equation (5) of the Appendix. Changing the sample temperature is the single most convenient

tool for affecting the UV damage rate. However, while we anticipate raising the temperature to help reduce the rate, it may also change the scaling regime. If pressure saturation had set in, for example, and the temperature is raised, the operating point may be moved out of the pressure saturated region so that the damage rate becomes again sensitive to the partial pressures. We would attempt to quantify the model well enough so that it could be used as a reliable predictive tool.

Finally, we would investigate the possible countermeasures which could be taken to reduce the rate of optics damage produced by UV irradiation. Increasing the temperature is one such approach. It is also possible to increase the partial pressure of O_2 in the vicinity of the optic. Oxygen molecules adsorbed on the surface may also be photolyzed by the UV, in which case they may react with the surface carbon, carrying it away to the pumps in the form of CO. If this process occurs with an appreciable rate constant, it could be very useful in inhibiting carbon buildup at the surface of the optic. We would attempt to measure the O_2 rate constants by observing the change in the degradation rates as a function of the O_2 partial pressure. Other means of reducing UV damage may also exist, and should be investigated.

With this information in hand, it will be possible to provide the first reliable scaling of the UV damage process to the free electron laser experiments. Given a knowledge of the photon energy band which causes the damage; the rates, saturation levels and fluences; and the pressure, intensity, and temperature

caling; one can calculate the anticipated damage rate in the high power tapered wiggler systems. Perhaps most important, these scaling relations and the identified countermeasures also allow the systems designer to select means which are effective in reducing UV induced absorption to tolerable levels.

c) Optical Samples

The optical coating materials to be used in the tests have been chosen according to the following criteria: a) they should include the most thoroughly characterized material SiO_2/TiO_2 in order to make contact with the available body of knowledge on optical materials performance; b) they should include materials which show a high fluence threshold to laser damage; and c), there should not be too many materials investigated so that the available experimental time is spent doing an in depth study learning new physics rather than doing a survey of many materials by measuring the same quantities over and over again.

Two coating methods have been chosen in priority as a result of the quality of the coatings produced (neutralized ion beam sputtering), and the widespread availability of the technique (e^- beam depostion). If additional time becomes available, it may be useful to examine CVD coatings and sol-gel coatings, but these techniques are not yet fully developed, and the UV quality of these coatings is more speculative.

The list of materials and their fabrication processes which

would be tested in the apparatus is given in Table II in approximate order of priority. A six month program would contcentrate exclusively on the SiO_2/TiO_2 samples, and on the Boeing witness plates.

SiO_2/TiO_2 + $\lambda/2$ SiO_2	ion beam sputtering
SiO_2/TiO_2	ion beam sputtering
SiO_2/TiO_2 + $\lambda/2$ SiO_2	e^- beam evaporation
SiO_2/TiO_2	e^- beam evaporation
SiO_2/ZrO_2	ion beam sputtering
SiO_2/ZrO_2 + $\lambda/2$ SiO_2	ion beam sputtering
SiO_2/ZrO_2	e^- beam evaporation
SiO_2/Sc_2O_3	either method
SiO_2/HfO_2	either method
SiO_2/Ta_2O_5	either method

Table II: Multilayer test materials and fabrication processes to be tested in the UV damage apparatus, in approximate order of priority.

3. Sample Introduction Chamber

a) Vacuum System Design

Drawing 10-0001 shows the permanently mounted portion of the chamber. The smaple holder is introduced into the existing ACO vacuum chamber by means of a long magnetic manipulator. It can be parked in the undulator beam on a support fixture while the manipulator is withdrawn and the gate valve is closed, isolating the storage ring vacuum from the sample introduction chamber. This precaution is necessary for vacuum safety.

Drawing 10-0004 is an end-on view of the existing vacuum chamber through the 8" flange. The offset of the mating flange places the sample holder in the only available space in the existing chamber, while maintaining the 12 mm stay-clear for the descending monochrometer beam. The "Stage I" components must be fabricated as early as possible. This section can only be mounted on the ACO vacuum chamber during a vacuum break of the FEL and VUV beamline apparatus which occur infrequently. We propose to fabricate this section and ship it to LURE for mounting on the next possible vacuum break. The rest of the chamber can be fabricated later and mounted onto the isolating gate valve without disturbing FEL operations.

Sheet 1 of drawing 10-0003 shows the side view of the sample introduction chamber. The manipulator mounts at right; it can pick off one of the samples stored on the carriage and move

it into the exposure position. The carriage moves on the track assembly so that different samples can be chosen from the group which happens to be loaded into the chamber at a given time. After exposure, the sample can be withdrawn and placed into the custom mirror mount assembly where the losses can be measured without an intervening exposure to air. The flexible orientation fitting allows the manipulator rod to be adjusted with respect to the vacuum chamber. The bellows assembly to the left allows the chamber to be aligned with respect to the Stage I assembly. Drawing 30-0007 shows the holdoff rods which prevent the bellows from collapsing when the vacuum is drawn.

Sheet 2 of drawing 10-0003 is the top view of the chamber. The sample carriage is shown loaded with twelve samples. This unit is actuated by a secondary manipulator and slides on rails transversely to the main manipulator. At right is the 6" gate valve which permits a loaded tray of samples to be installed into the carriage. Any sample can be withdrawn from the carrier by the main manipulator and inserted into the custom mirror mount assembly. A reference mirror is mounted in an identical assembly in the opposing position, forming the cavity for the in-situ ring-down loss measurement.

Drawing 30-0005 shows the pick-up head to be mounted onto the end of the main transfer rod. It will thread into a socket in the sample holder shown in drawing 30-0002 as the manipulator is rotated by its external magnetic actuator. Since the sample holder is mated with above its center of mass, it can neither

rotate nor fall off the manipulator arm. This screw-on arrangement provides a positive engagement between the feedthrough and the sample which is necessary for a fail safe transportation of the sample. For this purpose, the transfer rod used must be able to provide enough torque for the screw action. Although bellows-sealed linear motion feedthroughs can provide very high torque, the cost of this type of feedthrough with long travel range is quite high. Our colleagues at SSRL indicate that magnetically coupled feedthroughs which use samarium-cobalt permanent magnets, such as the ones made by Riber, can provide enough torque for our purpose with a more affordable price.

Galling is prevented by fabricating the pick-up head from BeCu and using stainless steel helicoil inserts in the sample holders which are fabricated from aluminum for lightness. Galling and sticking are prevented on the sliding base of the sample holders by fabricating the ways from stainless steel and coating the holder bases with MoS_2.

The pointed tip of the pick-up head guides it into the threaded socket in the sample holder despite vibrations of the 800 mm arm which will be in its full extended position when it picks up the sample holder inside the ring chamber. All parking positions for the sample holder (in the ring chamber, on the measurement mirror mount, and in the sample carrier), have vertical and horizontal ramps at the entry so that the insertion of the holder is facilitated. The holder is pinned against a reference surface by a BeCu spring in a groove.

Drawing 10-0006 shows the exterior of the vacuum chamber. Ports are provided for pumping, guages, and viewports at the areas where alignment is critical. Mounting tabs are provided for the optics which will bring the probe laser to the reference cavity, and for the chamber itself. The large flange at the bottom is for the cryopump; the small one for the forepumps.

The chamber and the components inside will be constructed of stainless steel. All flanges will be sealed with copper gaskets. With the exception of the isolation valve, all gate valves will have copper sealed bonnets and viton sealed gates.

b) Vacuum Pump Selection

The quality of the vacuum is a critical parameter in this experiment. Since the sample introduction chamber will open directly to the electron storage ring, the vacuum level in the chamber must reach the 10^{-10} torr range with low carbonaceous partial pressures before the connecting valve can be opened for sample introduction. To satisfy this requirement, we have selected an oil-free pumping system. A Venturi pump and three liquid-nitrogen chilled sorption pumps will be used to evacuate the system down to the millitorr range. The Venturi pump will substantially increase the useful life time of the sorption material between regeneration bakeouts. A cryopump with a closed-cycle helium gas refrigerator will pump the system down to

10^{-10} torr and hold it there during the experiment.

The size of the cryopump is determined by considering the desired base vacuum and the size of the chamber, reasonable pump down time and frequency of regeneration. We plan to use a Cryo-Torr-8 pump with an MC compressor made by CTI-Cryogenics. The pumping speed of this pump is 1500 liters/sec for air. Although this pump can run with a smaller compressor, the MC compressor offers enough capacity for running other cryopumps which will be required for the optional carbonaceous gas exposure experiment.

c) Loss Measurement System

As mentioned above, we have designed a means to perform the loss measurements in situ without the need to break the vacuum. Surface chemical contamination due to air exposure is completely eliminated in this system. Furthermore, since repeated pumpdowns are unnecessary, it will be possible to monitor the degradation much more frequently than with an ex-vacuo measurement system.

The layout of the optical loss measurement system shows how the cavity ringdown instrument would be interfaced to the in-vacuo resonator. The laser system and mode matching system will be mounted in a support structure adjacent to the chamber, and the beam injected into the chamber through optical quality windows. The photomultiplier is most conveniently mounted on the

optical table, but this means that it must be mounted behind a spatial filter to eliminate stray light. The ex-vacuo portion of the lossmeter will permit the optics to be characterized before insertion into the vacuum chamber.

The support structure will be designed and constructed on the site in order to adapt to the specific space constraints of the laboratory. We have sent the blueprints and description of our design to LURE for review and acceptance.

The estimated cost of the measurement system is $238,066. This includes both the vacuum system and the loss measurement system. See the Appendix for the parts list and detailed cost breakdown for these systems.

4. Carbonaceous Gas Test Chamber

The carbonaceous gas test chamber serves two principal functions. First, it provides the facility for introducing arbitrary gases into the vicinity of the optical sample, even though these gases may be strictly forbidden in the connecting storage ring vacuum system. Second, it includes appropriate ports for the surface analysis equipment which would be required to identify the electronic and structural interactions responsible for the induced optical losses.

Figure 4 shows the conceptual design of this chamber. (The final design remains to be performed.) It is intended to interface both with the ACO storage ring source and with the SPEAR WUNDER beamline. The gate valve at right mates with the existing storage ring flange; the undulator light enters from the right. In the case of ACO, the FEL mirror must be removed before this chamber can be installed. The NOEL UV beam passes through the FEL mirror holder, entering this chamber from the right. Unfortunately, the chamber must be dismounted so that the FEL mirror can be reinstalled each time a set of runs terminates.

In the case of SPEAR, this experiment can be permanently mounted into the "white light" section of beamline V. When this experiment is inactive, the undulator beam passes through the system and enters the existing monochrometer through the gate valve on the left.

The sample introduction chamber (beginning with Stage II) mates with the lateral gate valve towards the rear of the chamber. Ports are provided for the installation of a pair of reference mirrors which make possible the measurement of the evolution of the losses as a function of time during the exposure. Supplementary ports are provided for the mounting of surface diagnostic equipment such as XPS, a low energy electron gun, and a cylindrical electron momentum analyzer.

The chamber is divided into three sections to achieve the required level of differential pumping. The main chamber (a) is connected to the next (b) through a narrow tube of low conductance. The third chamber (c) becomes part of the beamline when the valve is opened, and is connected to (b) through an aperture of the same diameter as the tube. The aperture and the tube must be aligned with the undulator beam, so bellows are required at each end of the assembly, and an adjustment system must be incorporated into the support structure.

The main chamber (a) is pumped from below by an ion pump which can handle the high gas load. Pressures as high as 10^{-5} or even 10^{-4} Torr can be accommodated here. The buffer chamber (b) is pumped by a cryopump to obtain maximum isolation of the foreign gas pressure being introduced into the main chamber. The ion pump can be configured to pump both chambers in the holding mode when all cryopumps are shut down. The common manifold also permits rough pumping of the system. The manifold is gated off during differentially pumped operation. A thermocouple guage is

mounted in the manifold, and two ion guages are mounted in sections (a) and (b) of the chamber.

A gas manifold will be provided along with a calibrated leak valve for control of the partial pressure of the gases introduced into the main chamber.

The gas flow rate S (liter/s) from chamber (a) into chamber (b) through the tube is calculated from

$$S = C \frac{P_a - P_b}{P_a} \qquad (1)$$

where C is the conductance and P_a and P_b are the respective pressures. When the pressure differential is large enough, $S \simeq C$. The conductance of a cylincrical tube is given by

$$C = \frac{1}{4} \bar{v} A \left[1 + \frac{3L}{8R} \right] \qquad (2)$$

where $\bar{v}$ is the average velocity of the particles, A is the cross sectional area of the tube, L is its length, and R its radius. The average velocity is given by

$$\bar{v} = 1.46 \times 10^4 \sqrt{\frac{T}{M}} \quad (cm/s) \qquad (3)$$

where T is the temperature in Kelvin, and M is the Molar mass in g/mol.

If we choose the dimensions of the tube to be L = 3 cm and R = .4 cm, we find the conductance to be C = .21 liter/s (for CO). Let us take the worst case pressure in section (a) to be 10^{-5} or 10^{-4} Torr. The pressure in section (b) will be low enough so that the mass flow will be S = C = .21 liter/s.

The pressure in section (b) is given predominantly by the outgassing rate and the pumping rate. Using the post bakeout rate of stainless steel at 2×10^{-12} Torr·liter/s/cm^2, we find an outgassing flow of 10^{-8} Torr·liter/s assuming a 5000 cm^2 area for section (b). If we use another Cryotorr 8 cryopump with a 1500 liter/s pumping rate, we find a pressure of 6×10^{-12} Torr. Most importantly, the composition of the gas in section (b) is only .21/1500 = .01% composed of the foreign gas introduced in section (a). The flow rate of this gas into the storage ring vacuum (or into the beamline in the case of SPEAR) is then only 6×10^{-15} Torr·liter/s. This contaminant throughput should be low enough for any gas which is well pumped in the storage ring ion pumps.

5. Fabrication and Test Schedule

Figure 5 shows the schedule for the experiment. In view of the urgency of the need for UV damage information, we have done everything possible to accelerate the schedule. Fabrication and vacuum integrity testing will be complete at the end of the fourth month. Shipment to Orsay, the obligatory vacuum checkout by LURE, the fabrication of the support structure, and installation of the system consume another 4.5 months. We expect the first data to be taken in the ninth month from inception of the project. If the design of the carbonaceous gas chamber is complete at the beginning of the project, its fabrication could begin at any time before the start of the experiments depending on available cash flow, and be ready for operation at the end of the initial six month experimental period.

We believe 6 months of running time is the minimum required to answer the three basic questions listed at the top of Table I for the Boeing "burst mode" optics. If funds are available, the program should be extended to deal with the carbonaceous gas dependence, the alternative optical materials, and the countermeasures issues discussed in section 2 and Table I above.

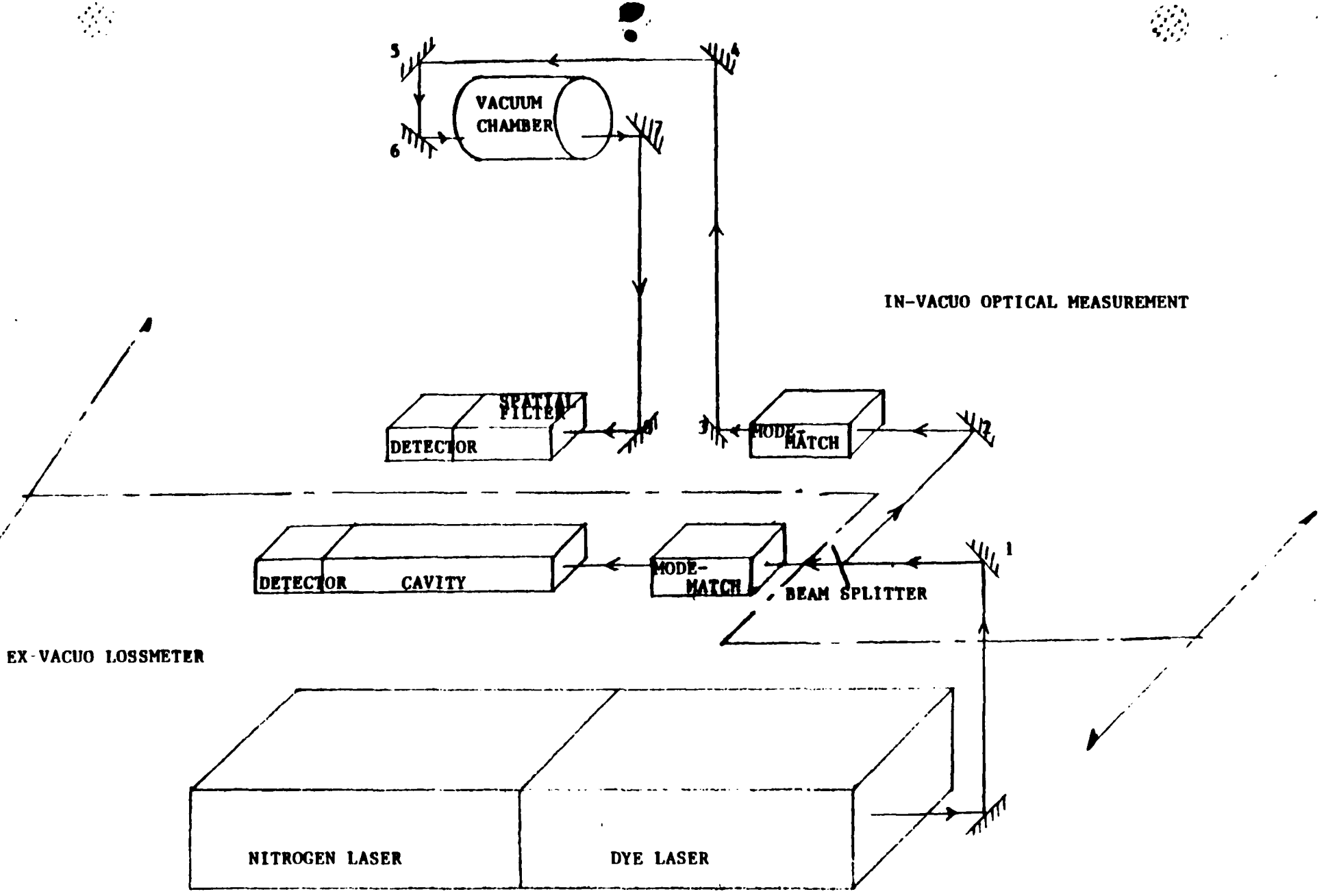

Figure 1:
Schematic Layout of the Optical Measurement System. 1-8 are beam steering system included in the cost estimate.

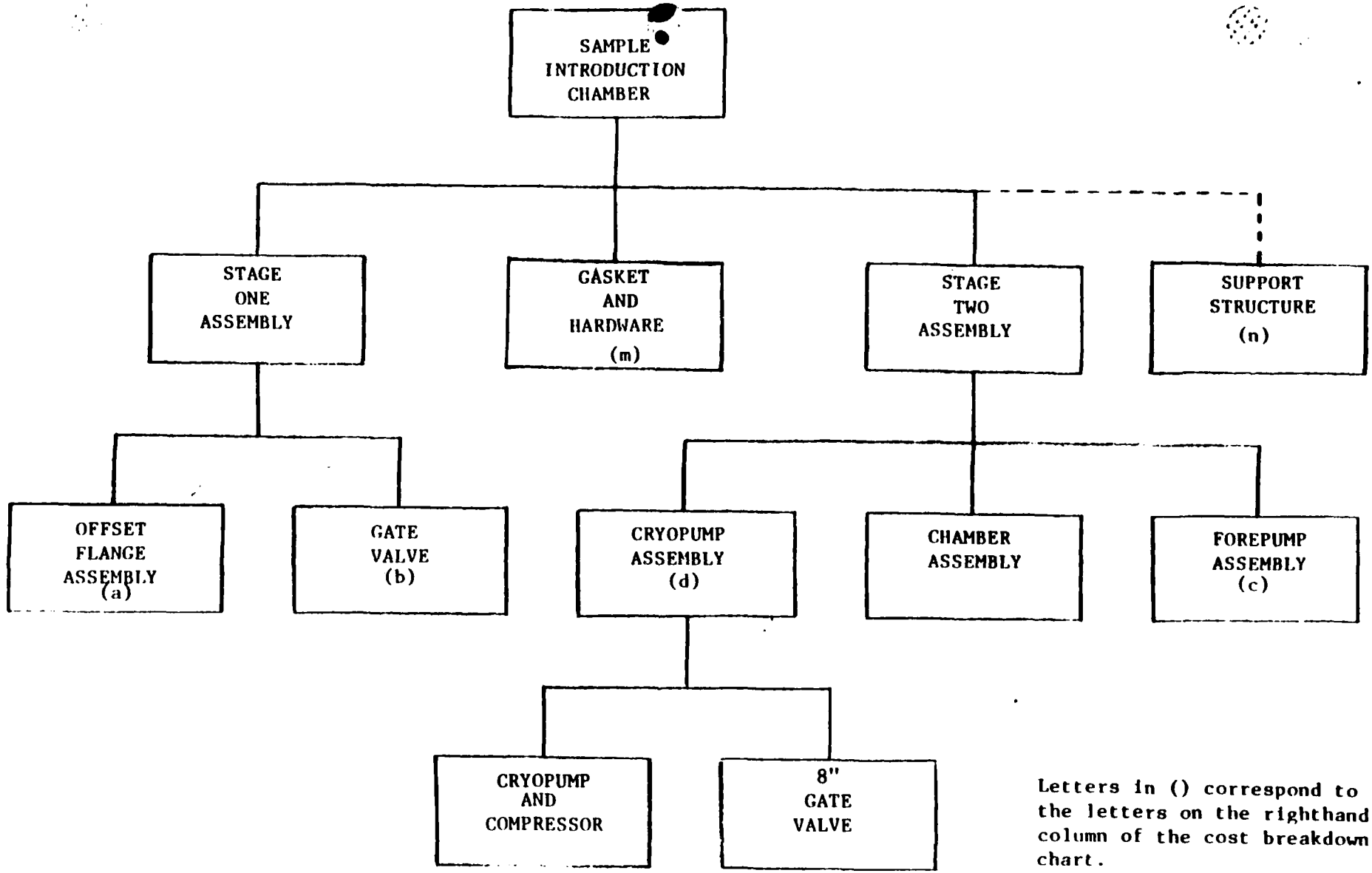

Letters in () correspond to the letters on the righthand column of the cost breakdown chart.

Figure 2:

Sample Introduction Chamber Assembly Chart.

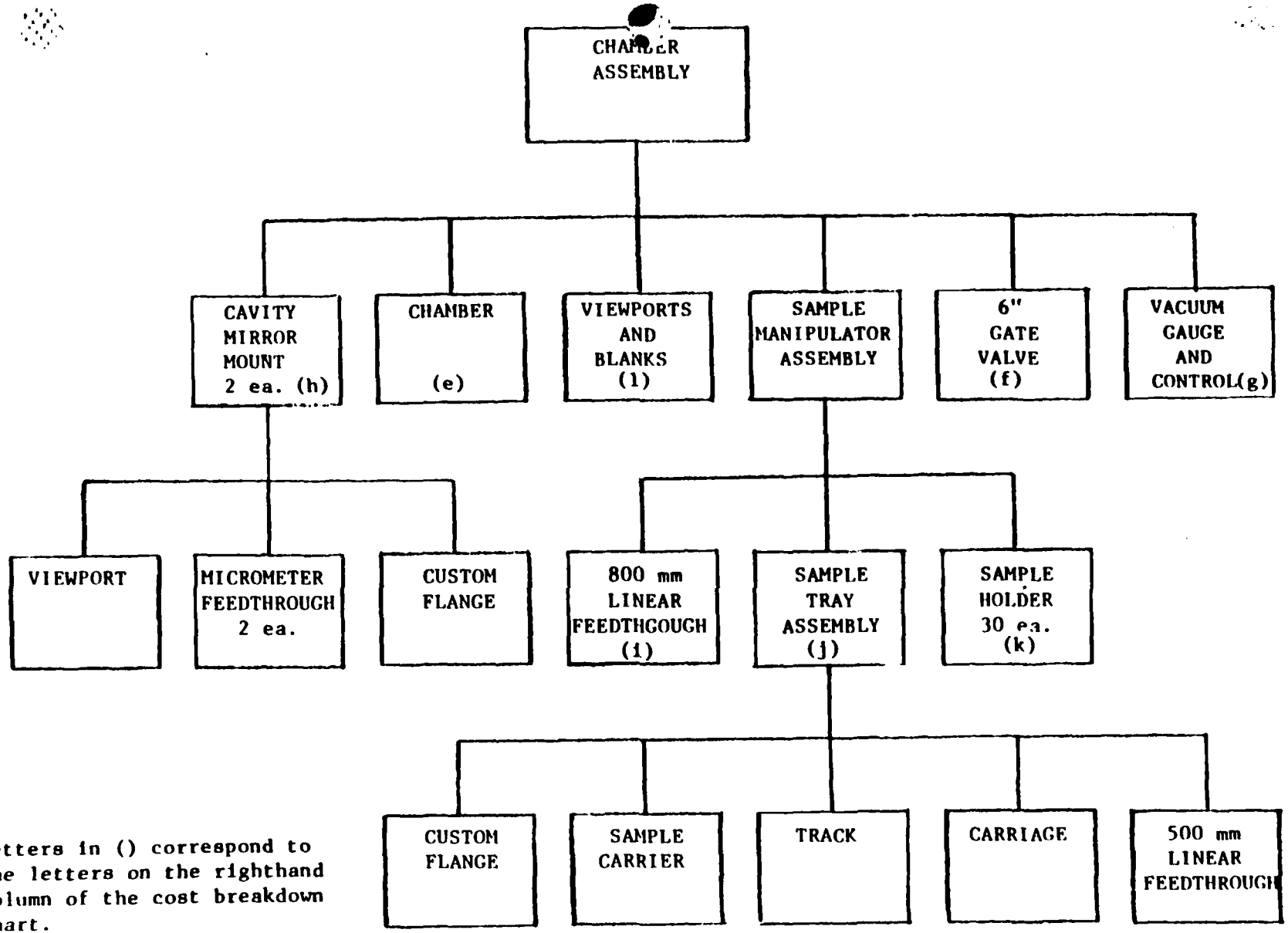

Letters in () correspond to the letters on the righthand column of the cost breakdown chart.

Figure 3: Chamber Assembly Detail

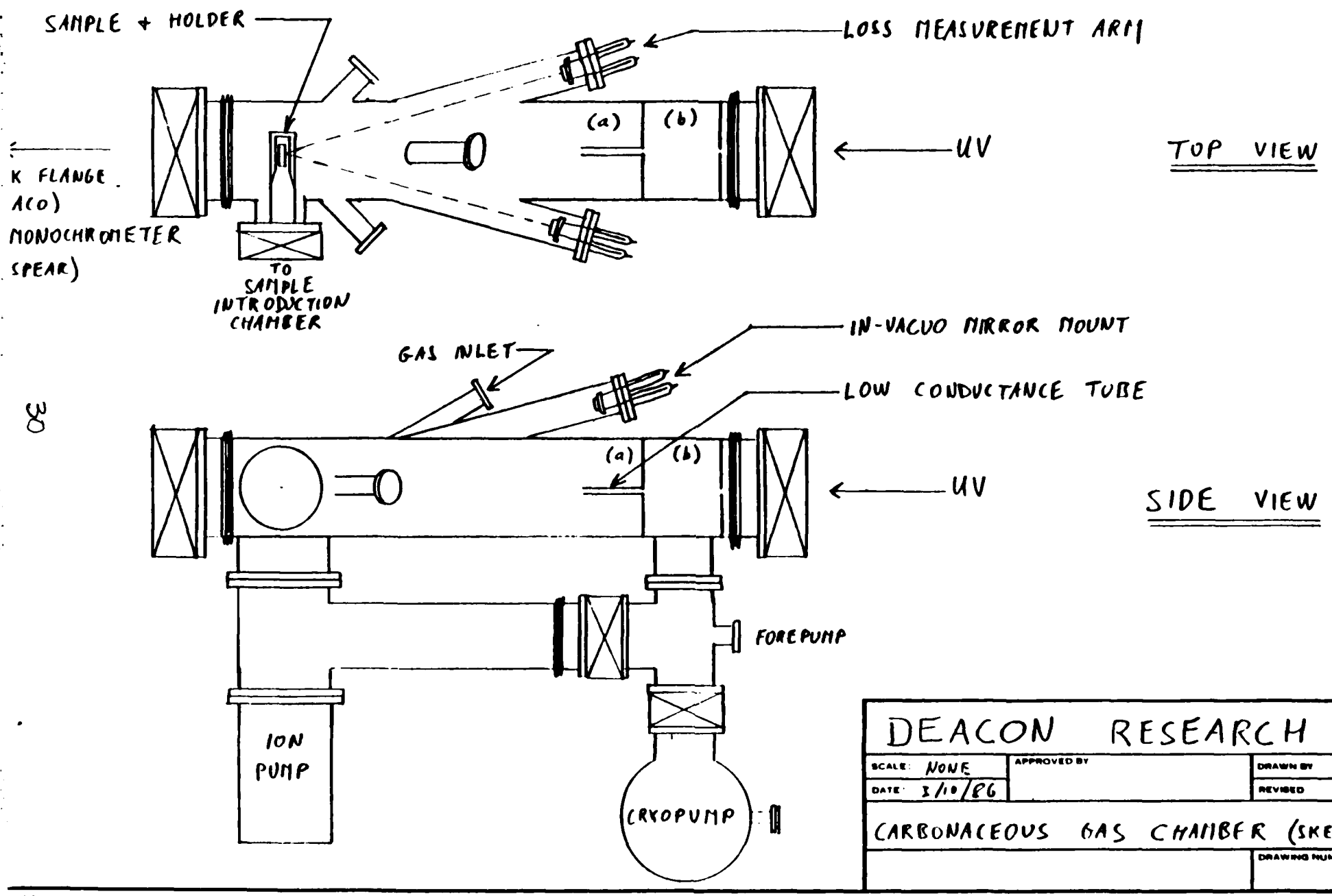
SAMPLE + HOLDER
LOSS MEASUREMENT ARM
(a)
(b)
UV
TOP VIEW
K FLANGE
ACO)
MONOCHROMETER
SPEAR)
TO
SAMPLE
INTRODUCTION
CHAMBER
IN-VACUO MIRROR MOUNT
GAS INLET
LOW CONDUCTANCE TUBE
(a)
(b)
UV
SIDE VIEW
FOREPUMP
ION
PUMP
CRYOPUMP
DEACON RESEARCH
SCALE: NONE
APPROVED BY
DRAWN BY D
DATE: 3/10/86
REVISED
CARBONACEOUS GAS CHAMBER (SKETCH)
DRAWING NUMBER

Figure 4

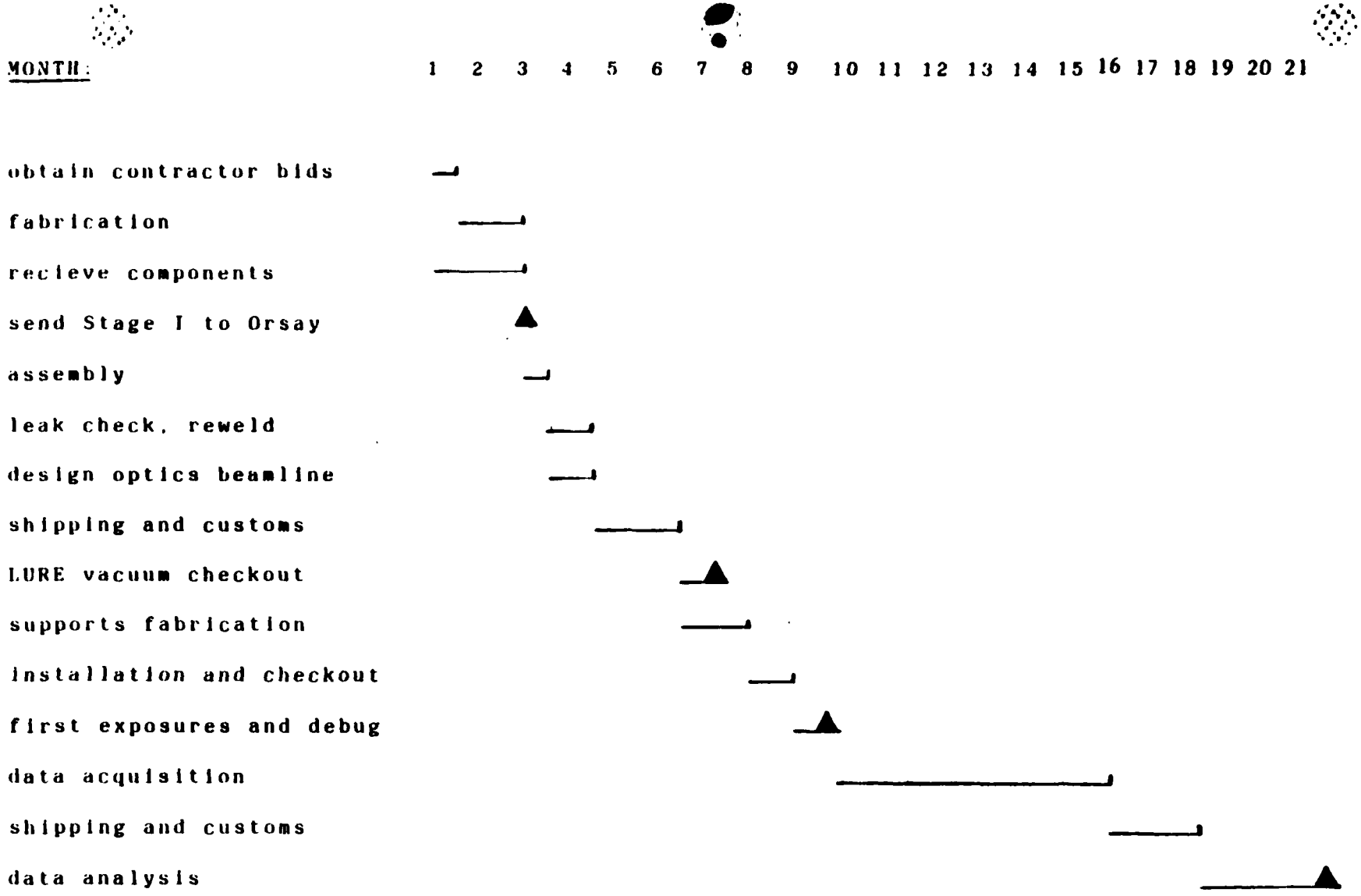

Figure 5. Schedule for the UV coating damage testing program.

Estimated Cost

of Capital Equipment For

FEL Optics Test Program

1. Sample Introduction Chamber	$ 88,850
2. Tunable Loss Measurement System	$ 149,216
TOTAL	$ 238,066

Estimated Cost Breakdown

I. Sample Introduction Chamber

Qty	Description	Vendor/Part #	Price	Total	
(i) Stage One Assembly					
1	8" Offset Flange with Sample Support Fixture	custom	1,000	$ 1,000	a
1	4" All-Metal Gate Valve	VAT 48044-CE01	6,812	6,812	b
(ii) Gaskets, Hardware, & Connectors				1,200	m
(iii) Stage Two Assembly					
	(1) Forepump Assembly				
3	Std Size VacSorb Pump	Varian 941-6501	1,560		
3	Liquid Nitrogen Dewar	Varian 944-0010	348		
3	Heating Band	Varian 944-0044	735		
3	Splash Shield	Varian 944-0007	294		
3	1.5" Viton Sealed Valve	Varian 951-5091	1,362		
1	1.5" Polyimide Sealed Valve	Varian 951-5092	799		
1	Back-to-Air Valve w/Flange	Varian 951-5097	230		
1	Venturi Pump w/Flange & TC	Varian 952-5095	572		
2	Nipple	Varian 952-5048	126		
2	Tee	Varian 952-5051	180		
2	Elbow	Varian 952-5049	126		
4	Hardware	Varian 953-5020	84		
2	Gaskets	Varian 953-5014	72		
			6,488	6,488	c
	(2) Cryopump Assembly				
1	CT-8 Pump with MC Compressor and Installation Kits	CTI-Cryogenic	12,010		
1	Regeneration Valve Assembly	US RVA-001MU	1,385		
1	8" O-Ring Sealed Gate Valve	MDC GV-8000M	3,550		
			16,945	16,945	d
	(3) Vacuum Chamber Assembly				
	* Cavity Mirror Mount Assembly				
2	Custom Mirror Mount	custom	2,000		
2	Custom 8" Flange	custom	1,000		
2	Saphire Viewport, 1.33"	MDC VP-075S	460		
4	Micrometer Feedthrough	Huntington VF-108	1,700		
			5,160	5,160	h
	*Custom Chamber				
1	Custom Chamber with Flanges	custom	7,500		
1	Bellows with 6" Flanges	Standard	1,500		
			9,000	9,000	e

	*Viewport and Blank-Offs				
2	8" Viewport	MDC VP-600	1,080		
1	6" Viewport	MDC VP-400	335		
7	2.75" Blank Flange	MDC F275000	98		
			1,513	1,513	i
	*Sample Manipulator Assembly				
	**800 mm Linear Motion Feedthrough				
1	Magnetically Coupled Transfer Rod, 800 mm Range	Riber TLTM 64-800	2,880		
1	Flexible Orientation Fitting	Riber RFO-64	1,280		
3	Custom Pick-Up Head	custom	150		
			4,310	4,310	j
	**Sample Tray Assembly				
1	8" Custom Flange	custom	375		
2	Sample Carrier	custom	2,000		
1	Rail Track	LinTech TRSA8-30 (modified)	400		
1	Carriage	custom	400		
1	Magnetically Coupled Transfer Rod, 500 mm Range	Riber TLTM 64-500	2,470		
			5,645	5,645	k
30	Sample Holder	custom	900	900	l
1	6" O-Ring Sealed Gate Valve	MDC GV-6000M	2,650	2,650	f
	* Vacuum Gauge and Control				
2	UHV Ionization Gauge Tube	Varian 971-5008	650		
2	Filament Repair Kits	Varian 971-0018	316		
1	Ionization Gauge & TC Control	Varian 0845-K8845-301	2,725		
1	Bakeable UHV Ion Gauge Cable	Varian 0891-K8845-310	322		
1	Auto Filament Turn-On and Over Pressure Protection	Varian 0891-K3128-301	210		
2	Thermocouple Guage Tubes	Varian 0531-F0472-303	96		
1	Residual Gas Analyzer	Leybold 901-001-G4	14,595		
			18,914	18,914	g
(iv)	Custom Support Structure	custom		2,500	n
	subtotal			$ 83,037	
	Sales Tax (7%)			5,813	
	TOTAL ESTIMATED COST OF SAMPLE INTRODUCTION CHAMBER			$ 88,850	

II. Tunable Loss Measurement System

Qty	Description	Vendor/Part #	Price	Total
	** Ex-Vacuo Loss Measurement System **			
1	Cavity Lossmeter, incl. 2" sample stage, λ scan, N_2 purge	DR	121,350	$121,350
1	Optical Table Breadboard 3' x 5'	NRC XS-35	1,800	1,800
1	Support Structure for above and lasers	custom	1,500	1,500
2	Cavity Mirrors (Spare)	DR	1,200	1,200
	** Add-ons for In-Vacuo Loss Measurement **			
	(1) Beam Splitter Assembly			
1	Broadband beam splitter	NRC 20B10.BS	261	
1	Mount for above	NRC 600A-2-S	175	
1	Rod & Clamp	NRC 340	118	
1	Variable Base	NRC VPB	108	
			662	662
	(2) Mode Matching Assembly			
2	Lens Holder	NRC MM-2A-B2	166	
1	Translation Stage	NRC 420-1-M	260	
2	Lens	OFR LLU-25	270	
1	Rod & Platform	NRC 300	191	
1	Variable Base	NRC VPB	108	
1	Custom adapter plate	custom	150	
			1,145	1,145
	(3) Beam Steering Assembly			
8	Mirror	NRC 20D04	664	
8	Mirror Holder	NRC 600A-2-S	1,400	
8	Rod & Clamp	NRC 70	944	
8	Rotatable Platform	NRC 34	640	
8	Variable Base	NRC VPB	864	
1	Custom Support Structure	custom	2,000	
1	Custom Beam Path Shield	custom	750	
			7,262	7,262
	(4) Cavity Mirrors			
2	Super Low Loss Mirrors	DR	1,200	1,200

	(5) Detector with Spatial Filter			
1	Photomultiplier	Hamamatsu 928	250	
1	PMT housing	Pacific 3150RF-S	275	
1	Custom Voltage Divider	custom	200	
1	Enclosure & Support	custom	750	
1	Cables & Hardware		100	
1	Spatial Filter	NRC 900	567	
1	Rod & Platform	NRC 300	191	
1	Variable Base	NRC VPB	108	
			2,441	2,441
	(6) Alignment Aids			
6	Iris	NRC ID-1.5	426	
6	Post	NRC SP-6	78	
6	Post Holder	NRC VPH-4	132	
6	Collar	NRC C-1	30	
6	Universal Base	NRC BU-P	228	
			894	894
	Subtotal			$139,454
	Sales Tax (7%)			9,762
	TOTAL ESTIMATED COST OF TUNABLE LOSS MEASUREMENT SYSTEM			$149,216

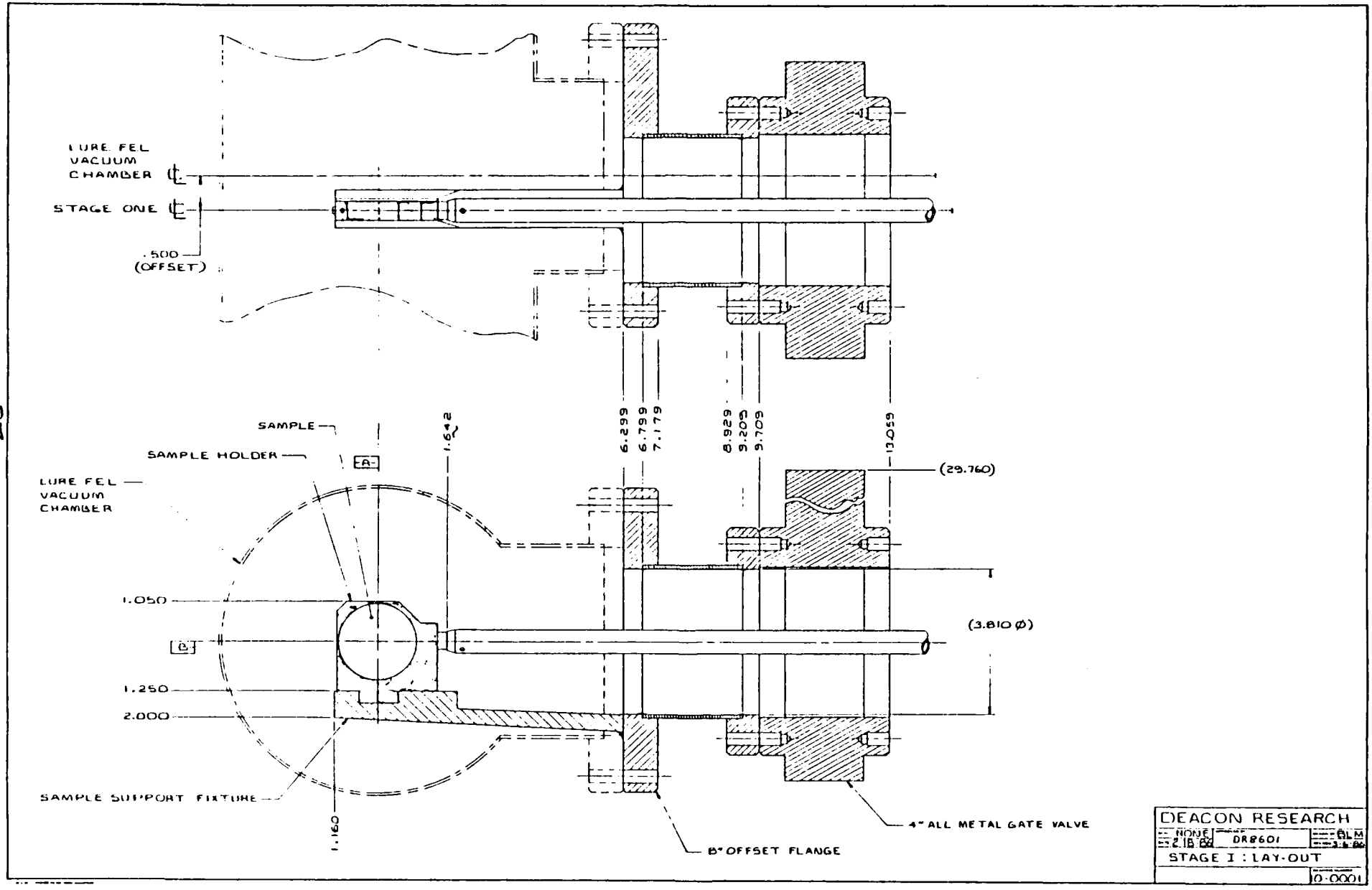
LURE FEL
VACUUM
CHAMBER
STAGE ONE
.500
(OFFSET)
SAMPLE
SAMPLE HOLDER
A
LURE FEL
VACUUM
CHAMBER
1.050
B
1.250
2.000
SAMPLE SUPPORT FIXTURE
1.160
1.642
6.299
6.799
7.179
8.929
9.205
9.709
13.059
(29.760)
(3.810 Ø)
4" ALL METAL GATE VALVE
8" OFFSET FLANGE
DEACON RESEARCH
NONE
2/8/86
DR8601
GLM
3/6/86
STAGE I : LAY-OUT
0-0001

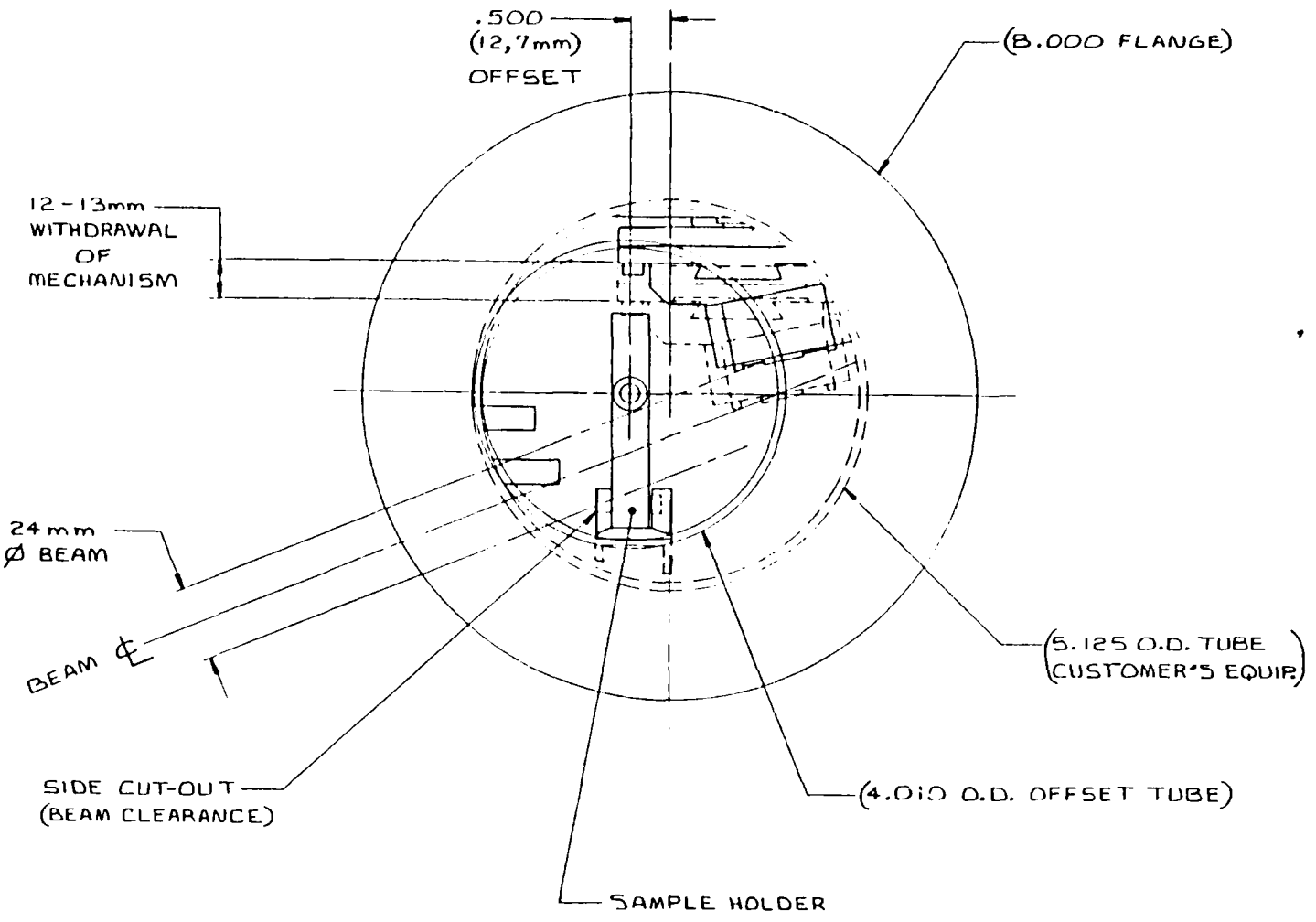

DEACON RESEARCH		
SCALE NONE	APPROVED BY DR 8601	DRAWN BY BLM
DATE 2-22-86		REVISED
SAMPLE POSITIONING		
		DRAWING NUMBER 10-0004

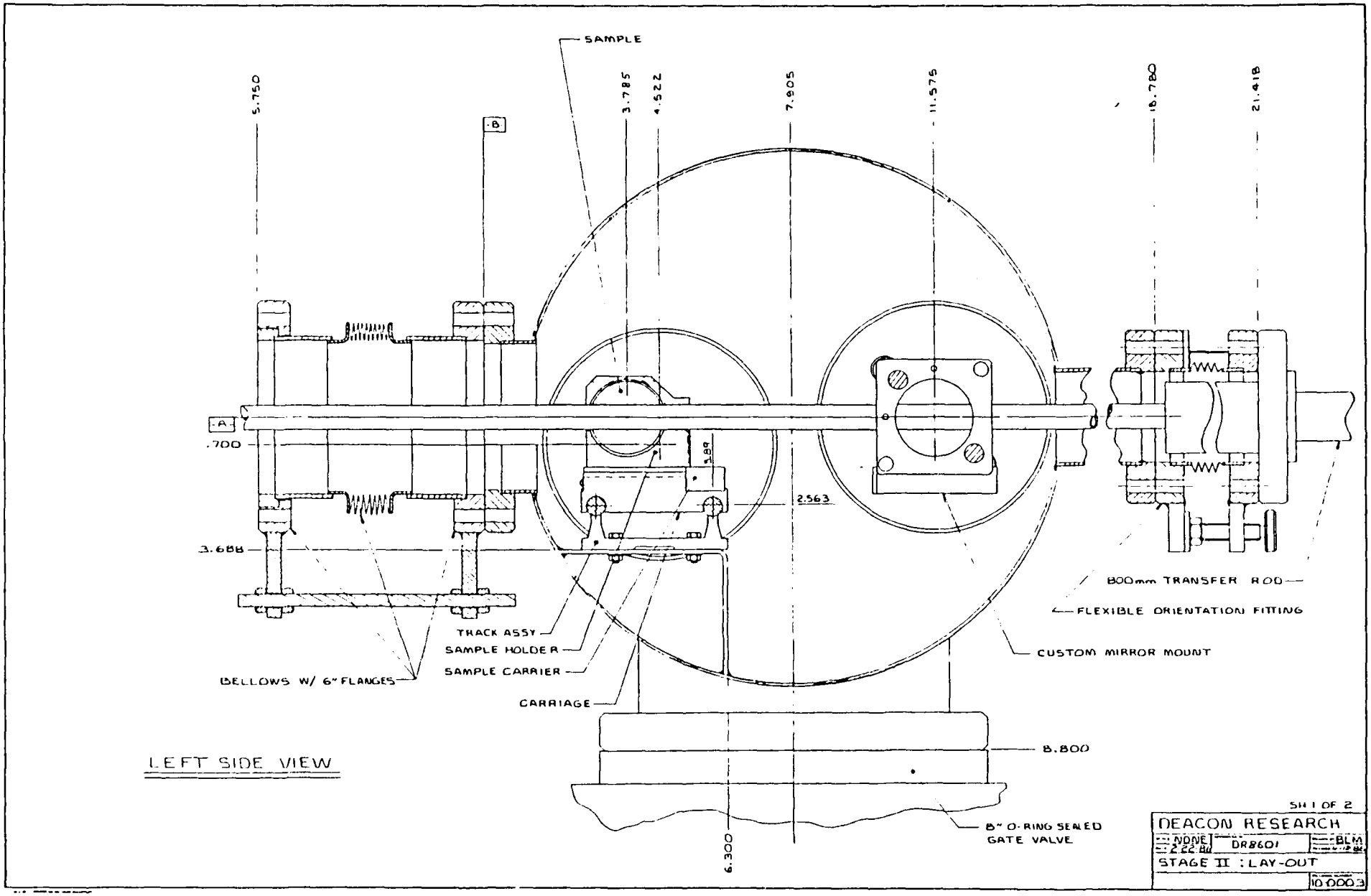
SAMPLE
5.750
3.785
4.522
7.905
11.575
16.780
21.418
B
A
.700
3.688
2.563
.89
800mm TRANSFER ROD
FLEXIBLE ORIENTATION FITTING
CUSTOM MIRROR MOUNT
TRACK ASSY
SAMPLE HOLDER
SAMPLE CARRIER
BELLOWS W/ 6" FLANGES
CARRIAGE
8.800
6.300
8" O-RING SEALED GATE VALVE
LEFT SIDE VIEW
SH 1 OF 2
DEACON RESEARCH
NONE
DR8601
BLM
STAGE II : LAY-OUT
10.0003

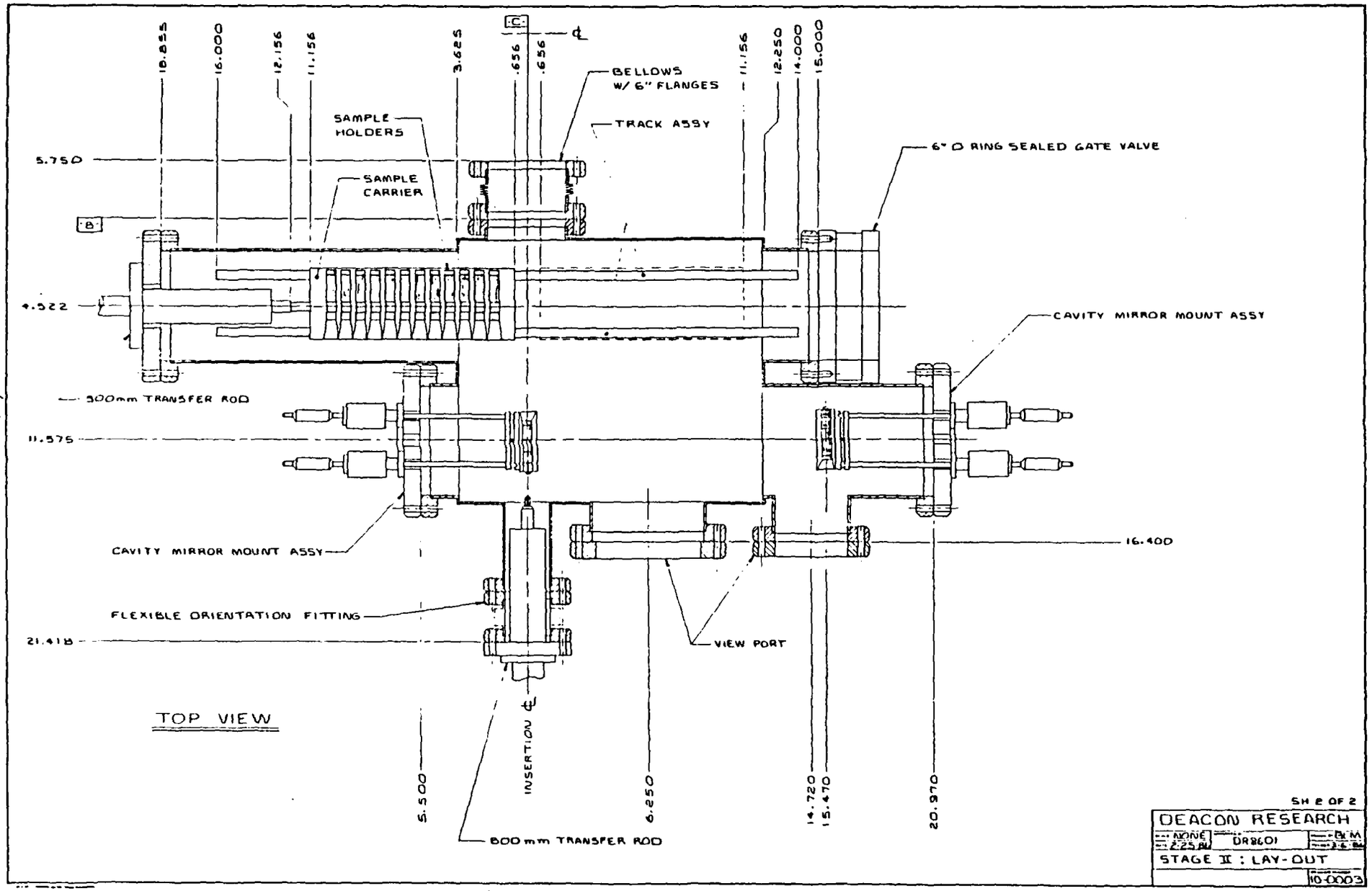

SH 2 OF 2

DEACON RESEARCH

NONE 2-25-81	DR2601	BY M

STAGE II : LAY-OUT

10-0003

NOTES (UNLESS OTHERWISE SPECIFIED):

1. THIS IS AN ULTRA-HIGH VACUUM COMPONENT.
2. USE OF SULFUR BEARING OILS OR ABRASIVES IS PROHIBITED.
3. WHEN MACHINING, USE ONLY CIMCOOL, KOOLMIST NO.77. OR MOBIL CUT-MAX.
4. ALL WELDS TO BE INSIDE, VACUUM TIGHT, TIG PROCESS & PERFORMED IN A CLEAN ROOM UNDER CONTROLLED CONDITIONS.
5. BREAK & DEBURR ALL SHARP EDGES & CORNERS.
6. CLEAN & DEGREASE & PACKAGE IN CLEAR PLASTIC PRIOR TO SHIPMENT.

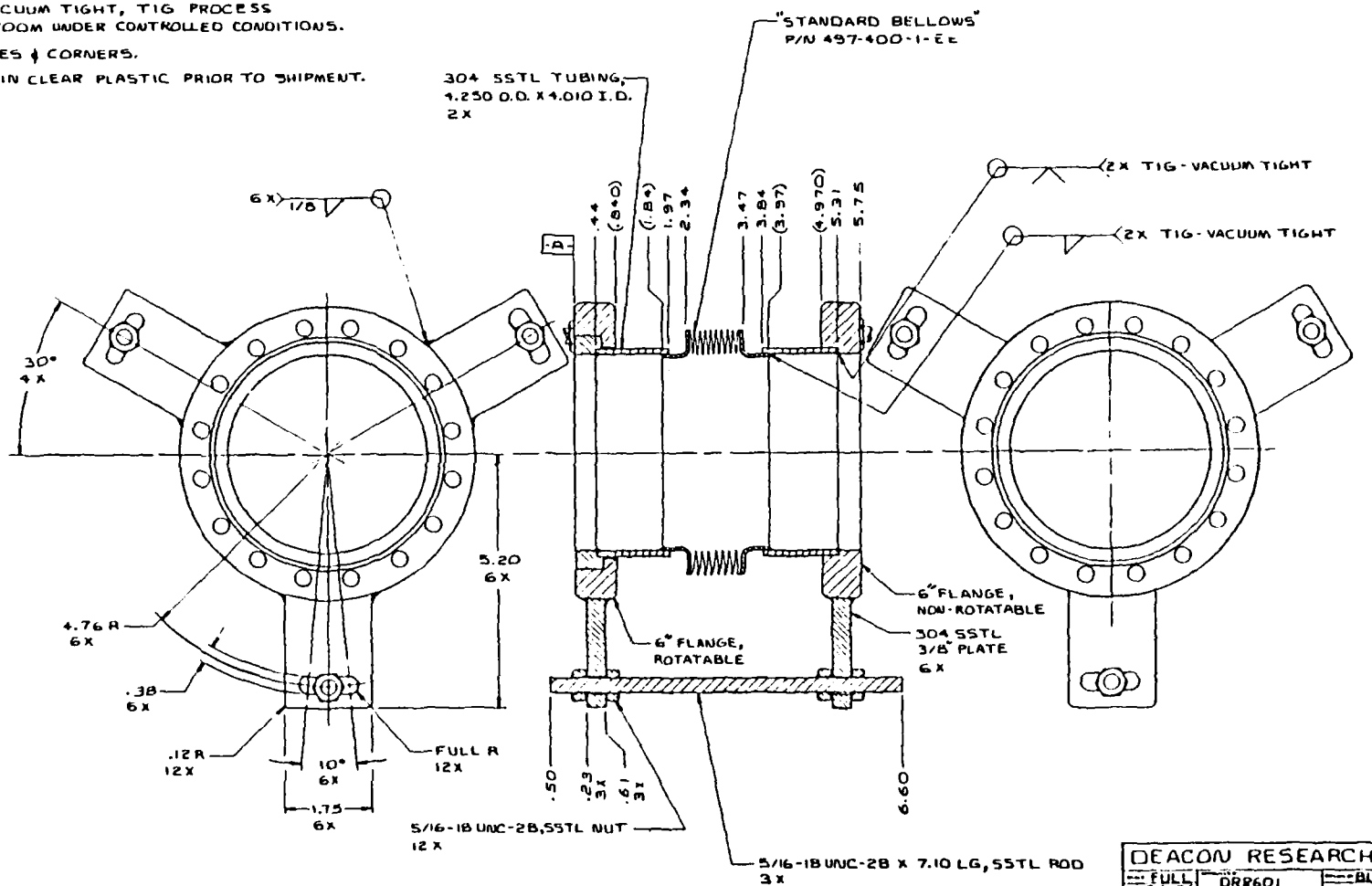

DEACON RESEARCH		
FULL	DRP601	BLM
TOL: .XX ± .01 ANG ± 1°	.XXX ± .005	
6" FLANGED BELLOWS	30-0007	

NOTES (UNLESS OTHERWISE SPECIFIED):

1. MATERIAL: BERYLLIUM COPPER, 25 HT ALLOY.
2. FINISH: NO. 63 OR BETTER ("MICROSEAL" 200-1 BY BY EM CORP. TO BE APPLIED THROUGH DEACON RESEARCH).
3. USE OF SULPHUR BEARING OILS AND ABRASIVES IS PROHIBITED.
4. USE CIMCOOL, KOOLMIST NO. 77 OR OR MOBIL CUT-MAX FOR LUBRICANT WHEN MACHINING.
5. BREAK & DEBURR ALL SHARP EDGES & CORNERS.
6. CLEAN & DEGREASE, PACKAGE IN CLEAR PLASTIC BAG AND MARK WITH P/N PRIOR TO SHIPMENT.

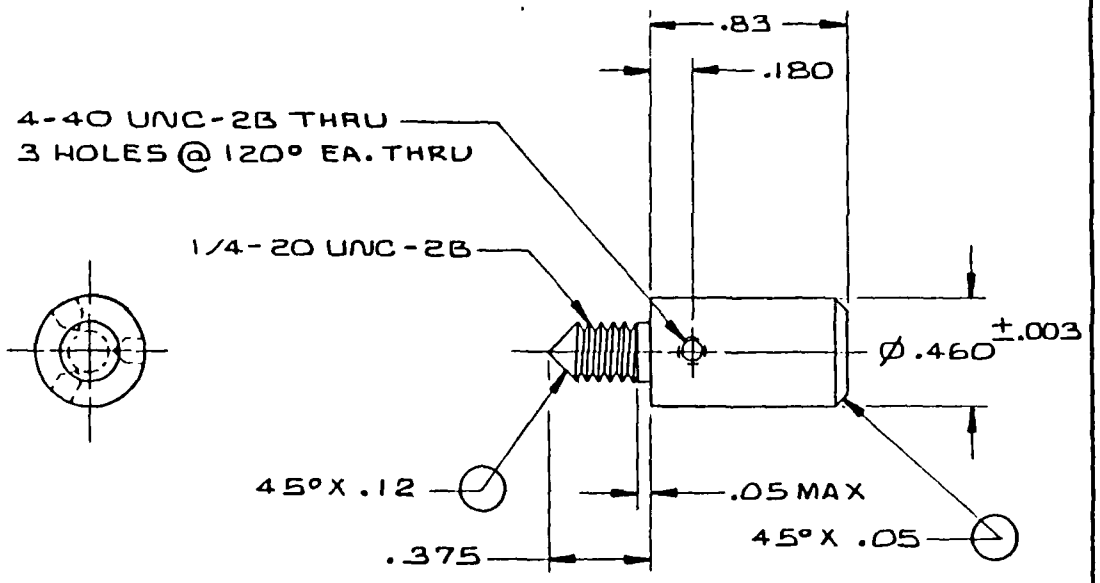

DEACON RESEARCH		
SCALE 2/1	APPROVED BY DR8601	DRAWN BY BLM
DATE 2-22-86		REVISED
TOL: .XX = ±.01 .XXX = ±.005 ANG. = ±1°		
PICK-UP HEAD		DRAWING NUMBER 30-0005

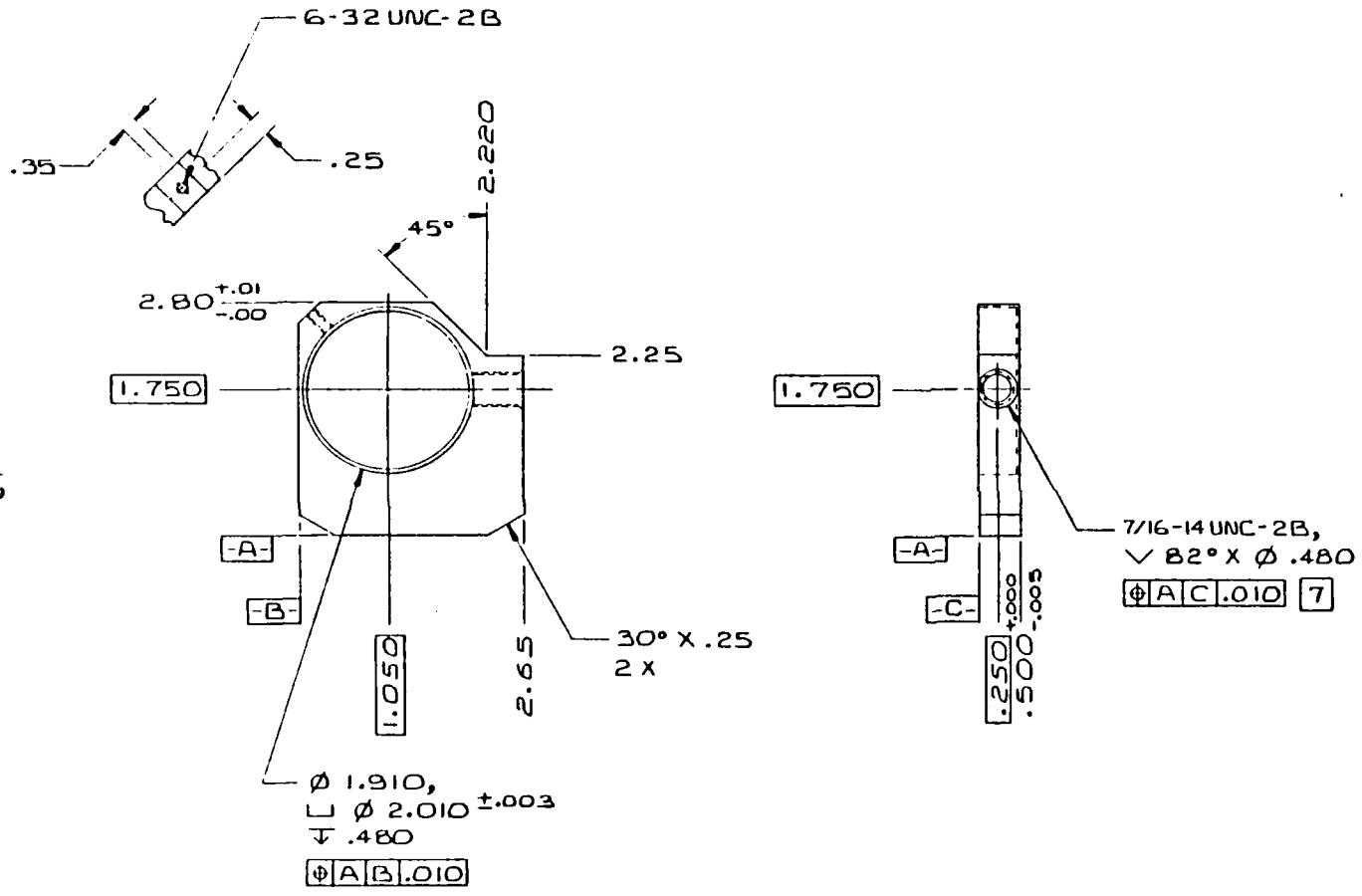

NOTES (UNLESS OTHERWISE SPECIFIED):

1. MATERIAL: ALU ALLOY, 6061-T6
2. FINISH: NO. 63 OR BETTER ("MICROSEAL" 200-1 BY EM CORP. TO BE APPLIED THROUGH DEACON RESEARCH).
3. USE OF SULPHER BEARING OILS & ABRASIVES IS PROHIBITED.
4. USE CIMCOOL, KOOLMIST NO. 77 OR MOBIL CUT-MAX FOR LUBRICANT WHEN MACHINING.
5. BREAK & DEBURR ALL SHARP EDGES & CORNERS.
6. CLEAN, DEGREASE, PACKAGE IN CLEAR PLASTIC BAG AND MARK BAG WITH P/N PRIOR TO SHIPMENT.
7. INSTALL 1/4-20 UNC-2B SSTL THREADED INSERT AFTER ULTRASONIC CLEANING (TO BE PERFORMED BY DEACON RESEARCH).

DEACON RESEARCH		
SCALE FULL	APPROVED BY DR 8601	DRAWN BLM
DATE 2-18-86		REVISED
TOL: .XX ± .01 .XXX ± .005 ANG. ± 1°		
SAMPLE HOLDER	30	DRAWING NUMBER -0002

NOTES (UNLESS OTHERWISE SPECIFIED):

1. MATERIAL: RAW STOCK & TUBING TO BE 304 SSTL. FLANGES TO BE "CONFLAT" TYPE, CROSS FORGED, 304 SSTL.
2. FINISH: ELECTRO-POLISH.
3. THIS IS AN ULTRA HIGH VACUUM COMPONENT.
4. USE OF SULFUR BEARING OILS OR ABRASIVES IS PROHIBITED.
5. WHEN MACHING USE ONLY CIMCOOL, KOOLMIST NO.77 OR MOBIL CUT-MAX.
6. ALL WELDS TO BE INSIDE (EXCLUDING EXTERNAL BRACKETS), VACUUM TIGHT TIG PROCESS PERFORMED IN A CLEAN ROOM UNDER CONTROLLED CONDITIONS.

[7] FLANGES INDICATED ARE TO BE ORIENTED AS SHOWN IN DETAIL [10].

8. BREAK & DEBURR ALL SHARP EDGES & CORNERS.
9. CLEAN & DEGREASE. PACKAGE IN CLEAR PLASTIC (SEALED) PRIOR TO SHIPMENT.

[10] AFTER FLANGE SPECIFIED IN KEY IS INSTALLED, CAP WITH A BLANK FLANGE & GASKET AND SEAL.

FLANGE KEY

ITEM	FLANGE SIZE & DESCRIPTION	TUBING SIZE, OD X ID	BLANKED [10]
(1)	10" NON-ROT.	8.020 X 7.810	
(2)	8 NON-ROT.	6.020 X 5.810	
(3)			
(4)	[7]		
(5)			
(6)	[7]		
(7)	8" NON-ROT.	6.020 X 5.810	
(8)	6" NON-ROT. TAPPED [7]	4.010 X 3.810	
(9)	6" NON-ROT.	4.010 X 3.810	
(10)	4-1/2" NON-ROT.	2.510 X 2.375	
(11)	2-3/4 NON-ROT.	1.510 X 1.375	YES
(12)			
(13)			
(14)			
(15)			
(16)			
(17)			
(18)	2-3/4 NON-ROT.	1.510 X 1.375	YES

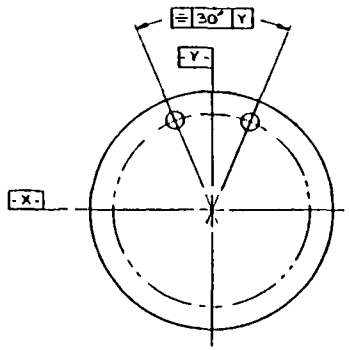

DETAIL [10] [7]
SCALE: NONE

SH 1 OF 3

DEACON RESEARCH		
--- 1/4	DR8601	---BLM
--- 3.15 PM		
TOL: .X ± .06 .XX ± .01 ANG ± 30'	.XXX ± .005	
MAIN TEST CHAMBER	30-0012	

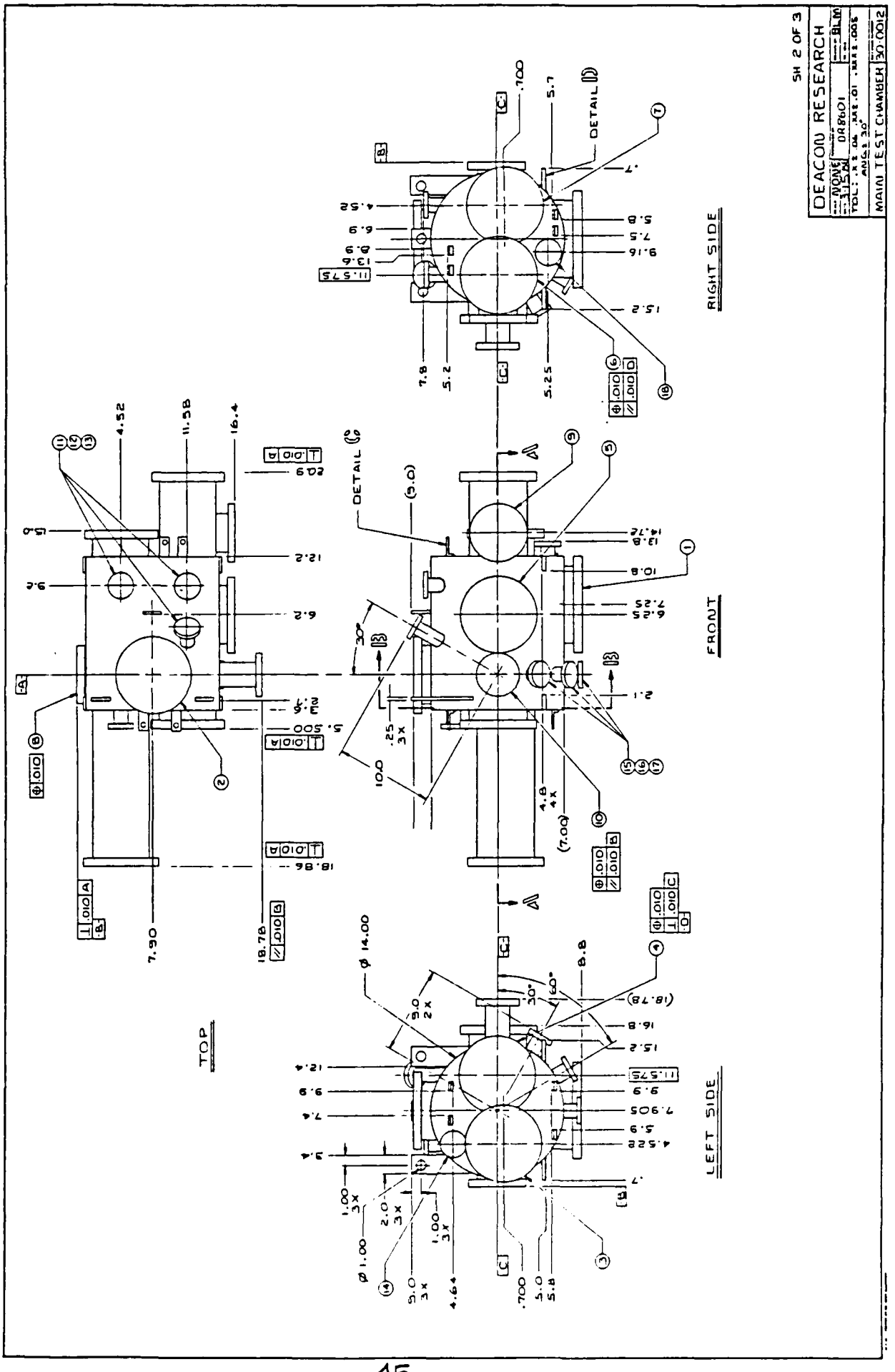
DEACON RESEARCH
DR8601
MAIN TEST CHAMBER
SH 2 OF 3
TOP
FRONT
RIGHT SIDE
LEFT SIDE
DETAIL
DETAIL

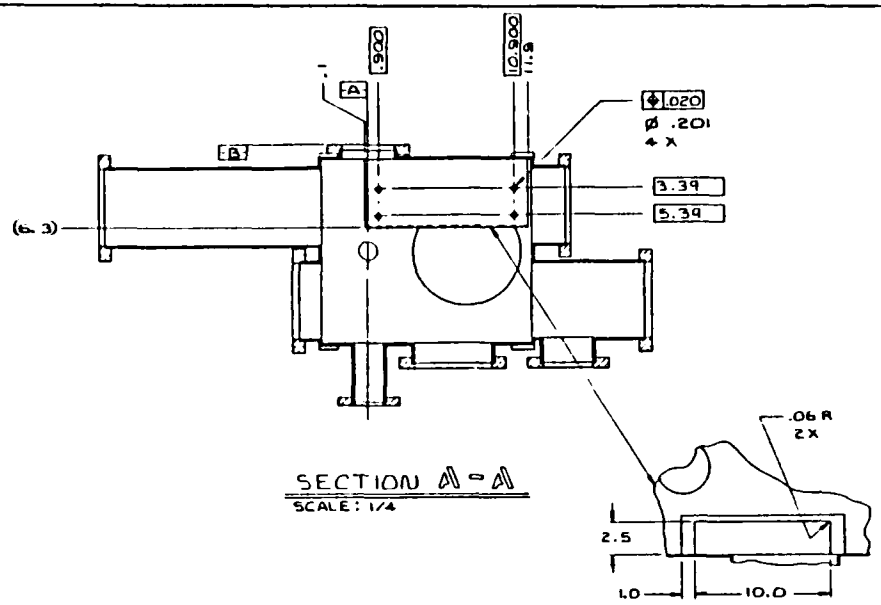

SECTION A-A
SCALE: 1/4

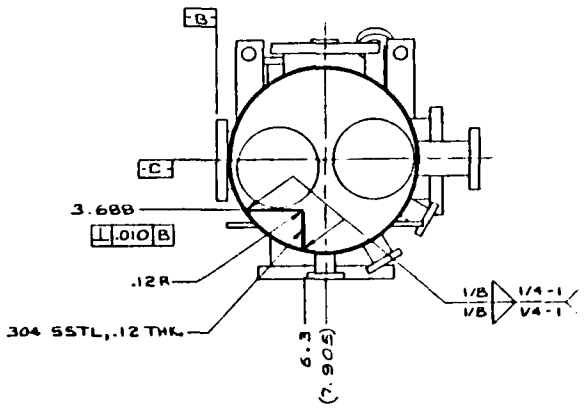

SECTION B-B
SCALE: 1/4

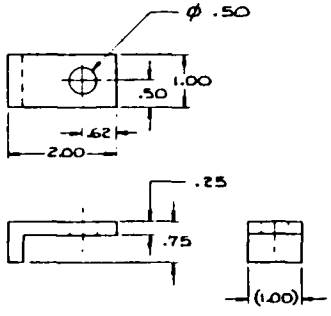

DETAIL C
SCALE: FULL 8X

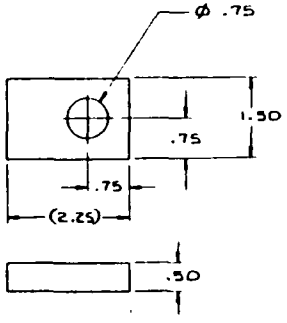

DETAIL D
SCALE: FULL 4X

SH 3 OF 3

DEACON RESEARCH		
1/4	DR8601	BLM
3.15 PM		
TOL: .X ± .06 .XX ± .01 .XXX ± .005 ANG. ± 30'		
MAIN TEST CHAMBER	30-0012	

NOTES (UNLESS OTHERWISE SPECIFIED):

1. MATERIAL: 304 SSTL
2. FINISH: NO. 63 OR BETTER ("MICROSEAL" 200-1 BY EM CORP. TO BE APPLIED THROUGH DEACON RESEARCH).
3. THIS IS AN ULTRA HIGH VACUUM COMPONENT.
4. USE OF SULFUR BEARING OILS OR ABRASIVES IS PROHIBITED.
5. WHEN MACHINING, USE ONLY CIMCOOL, KOOLMIST NO. 77 OR MOBIL CUT-MAX.
6. BREAK & DEBURR ALL SHARP EDGES & CORNERS.
7. CLEAN & DEGREASE & PACKAGE IN CLEAR PLASTIC BAG PRIOR TO SHIPMENT.

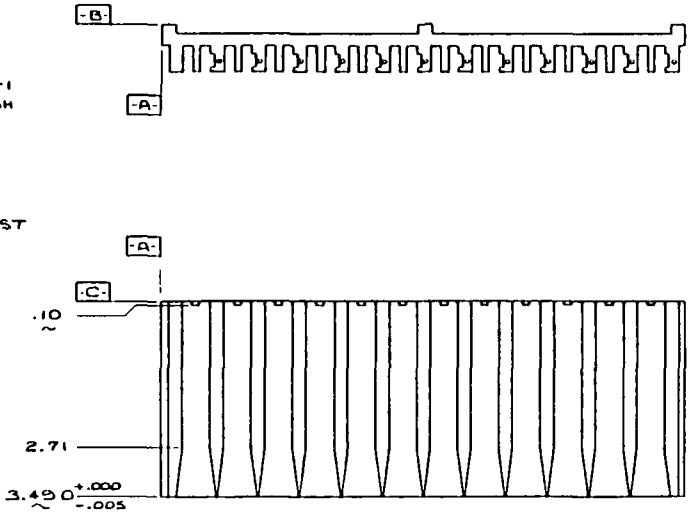

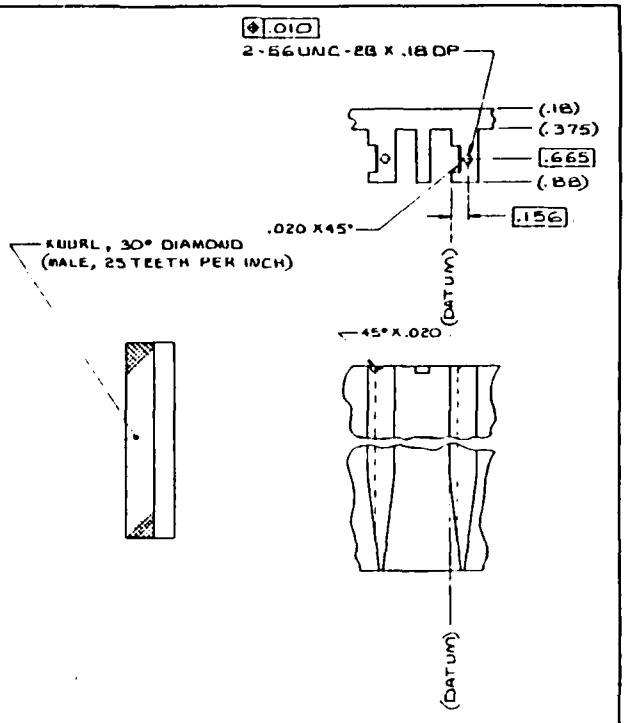

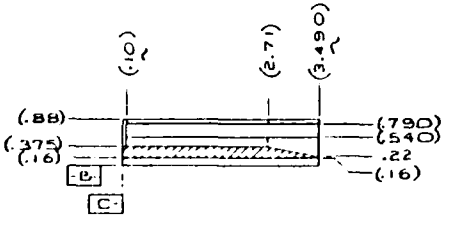

SECTION A-A
FULL 12 X

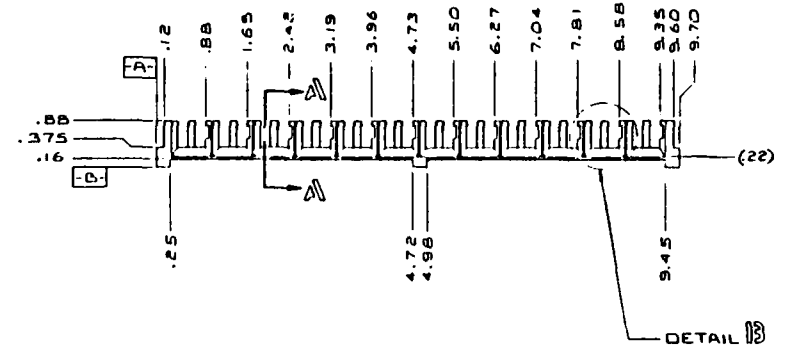

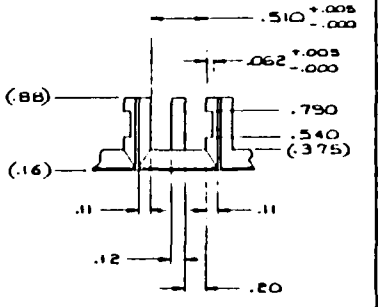

DETAIL B
2/1 12X

DEACON RESEARCH		
FULL 3 12 6	DR8601	SLM
SAMPLE CARRIER		

NOTES (UNLESS OTHERWISE SPECIFIED):

1. MATERIAL: ALU ALLOY, 6061-T6.
2. FINISH: NO. 63 OR BETTER ("MICROSEAL" 200-1 BY EM CORP. TO BE APPLIED THROUGH DEACON RESEARCH).
3. THIS IS AN ULTRA HIGH VACUUM PRODUCT.
4. USE OF SULFUR BEARING OILS OR ABRASIVES IS PROHIBITED.
5. WHEN MACHING, USE ONLY CIMCOOL, KOOLMIST NO. 77 OR MOBIL CUT-MAX.
6. BREAK & DEBURR ALL SHARP EDGES & CORNERS.
7. CLEAN & DEGREASE AND PACKAGE IN CLEAR PLASTIC PRIOR TO SHIPMENT.

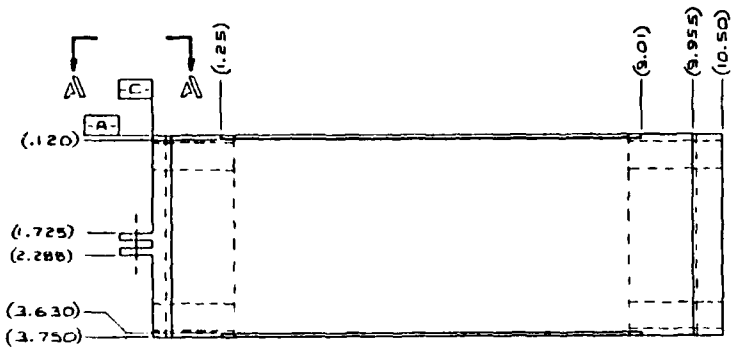

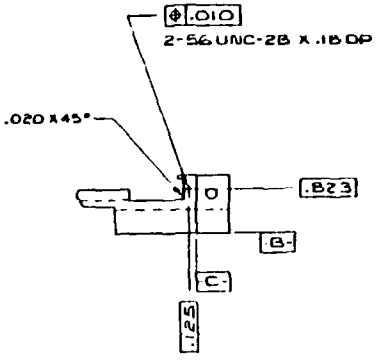

VIEW A-A
FULL
(ROTATED CW 180°)

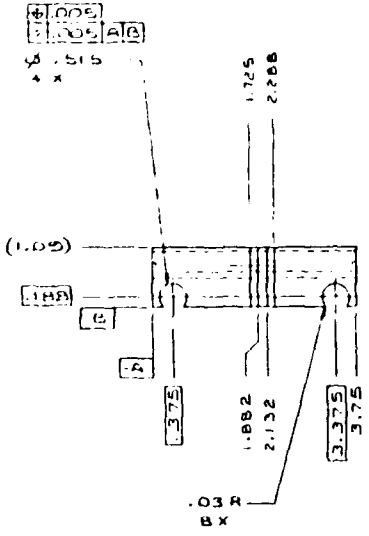

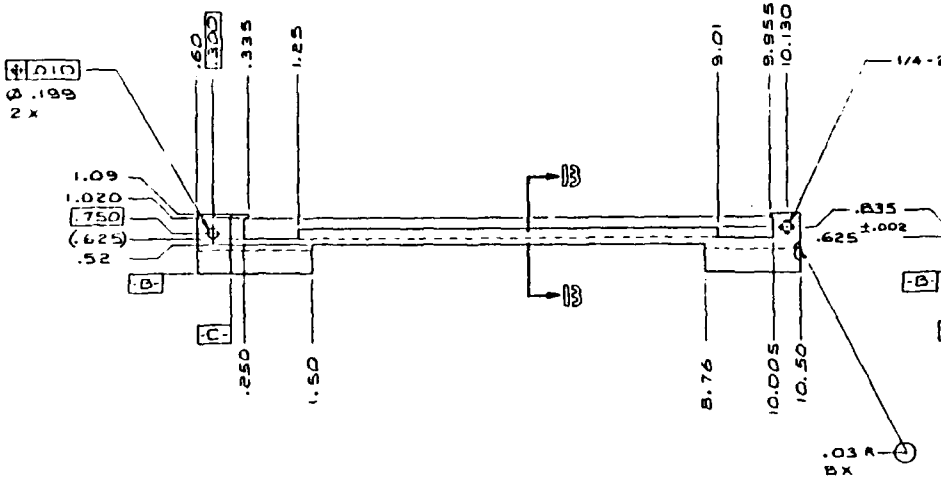

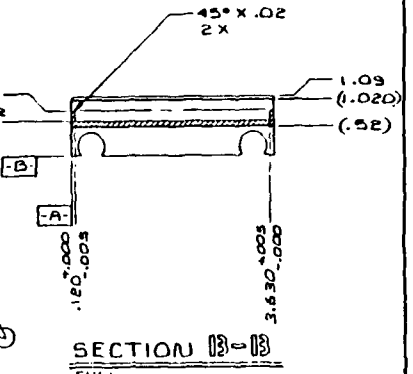

SECTION 13-13
FULL

DEACON RESEARCH		
FULL / 3:1 / B	DRB601	BLM
TOL: .XX ± .01 .XXX ± .005 ANG ± 1°		
CARRIAGE		

48

NOTES (UNLESS OTHERWISE SPECIFIED):

1. MATERIAL: 304 SSTL
2. FINISH: NO. 63 OR BETTER ("MICROSEAL" 200-1 BY EM CORP. TO BE APPLIED THROUGH DEACON RESEARCH).
3. USE OF SULFUR BEARING OILS AND ABRASIVES IS PROHIBITED.
4. WHEN MACHINING USE CIMCOOL, KOOLMIST NO.77 OR MOBIL CUT-MAX FOR LUBRICANT.
5. BREAK & DEBURR ALL SHARP EDGES & CORNERS.
6. CLEAN & DEGREASE & PACKAGE IN CLEAR PLASTIC BAG PRIOR TO SHIPMENT.

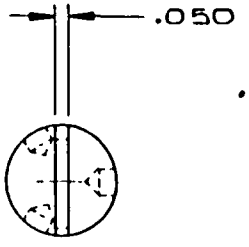

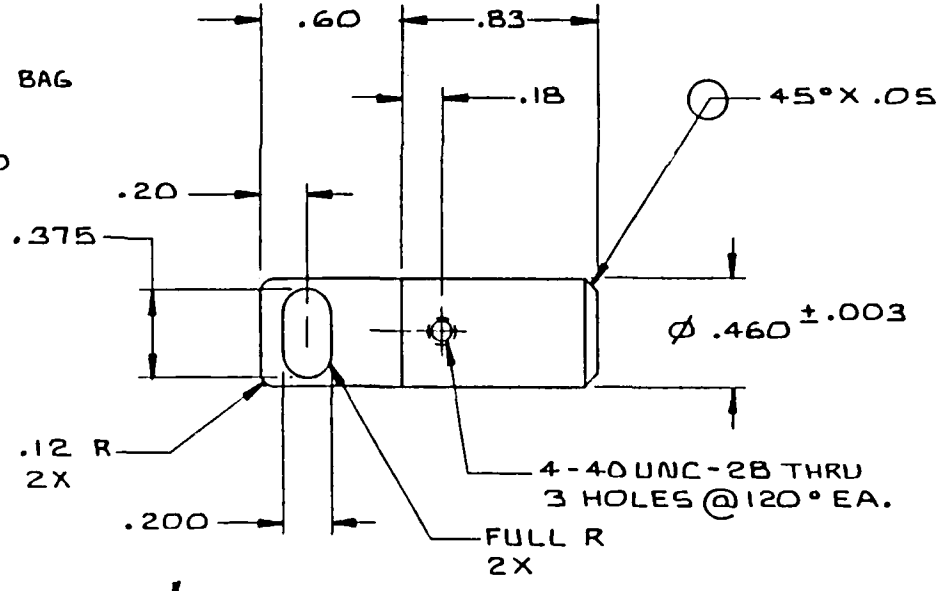

DEACON RESEARCH		
SCALE 2/1	APPROVED BY: DR8601	DRAWN BY BLM
DATE 3-13-86		REVISED
TOL: .XX ±.01 .XXX ±.005 ANG. ±1°		
CARRIAGE LINK		DRAWING NUMBER 30-0010

NOTES (UNLESS OTHERWISE SPECIFIED):

1. THIS IS AN ULTRA HIGH VACUUM COMPONENT.
2. USE OF SULFUR BEARING OILS OR ABRASIVES IS PROHIBITED.
3. WHEN MACHINING USE ONLY CIMCOOL, KOOLMIST NO.77 OR MOBIL CUT-MAX.
4. ALL WELDS TO BE INSIDE, VACUUM TIGHT, TIG PROCESS & PERFORMED IN A CLEAN ROOM UNDER CONTROLLED CONDITIONS.
5. FINISH SAMPLE SUPPORT FIXTURE NO.63 OR BETTER("MICROSEAL" 200-1 BY EM CORP. TO BE APPLIED THROUGH DEACON RESEARCH AFTER FIXTURE IS WELDED INTO PLACE: FLANGES TO BE PROTECTED DURING APPLICATION OF "MICROSEAL").
6. BREAK & DEBURR ALL SHARP EDGES & CORNERS.
7. CLEAN & DEGREASE & PACKAGE IN CLEAR PLASTIC PRIOR TO SHIPMENT.

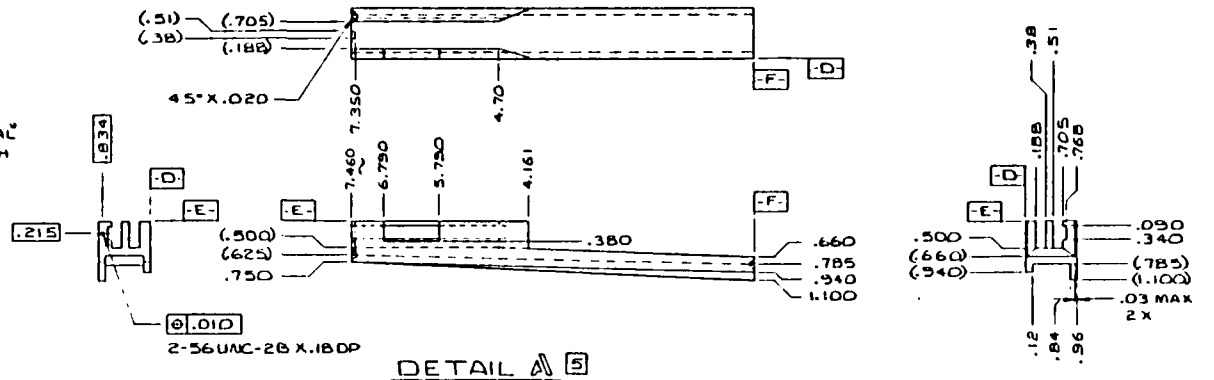

DETAIL A 5
FULL
SAMPLE SUPPORT FIXTURE
MAT'L: 304 SSTL

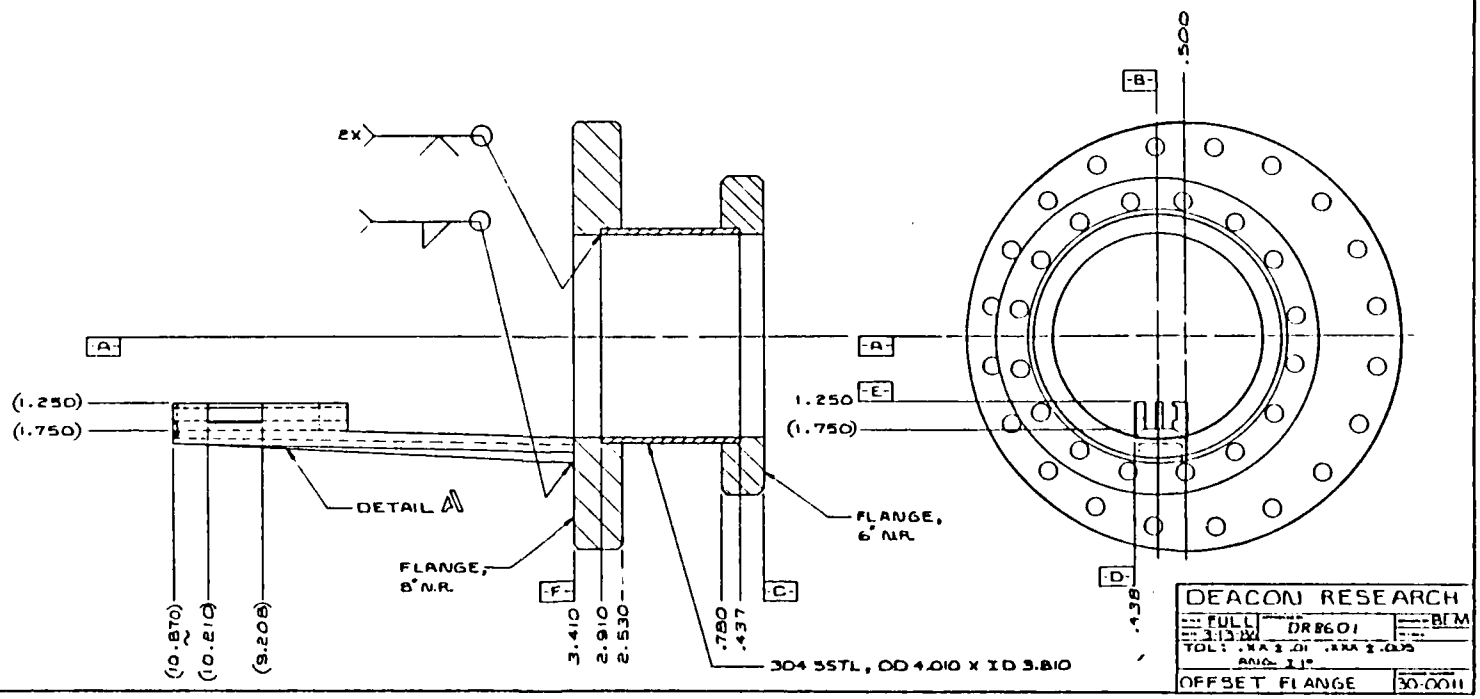

DEACON RESEARCH		
FULL 3:1 SCALE	DR8601	BEM
TOL: .XX ± .01 .XXX ± .005 ANG: ± 1°		
OFFSET FLANGE		30-0011

50

NOTES (UNLESS OTHERWISE SPECIFIED):

1. MATERIAL: 304 SSTL CROSS-FORGED CONFLAT (OR EQUIV.) FLANGE, 8" Ø, BLANK.
2. FINISH: ELECTROPOLISH.
3. THIS IS AN ULTRA HIGH VACUUM COMPONENT.
4. USE OF SULFUR BEARING OILS OR ABRASIVES IS PROHIBITED.
5. WHEN MACHINING USE ONLY CIMCOOL, KOOLMIST NO.77 OR MOBIL CUT-MAX.
6. PROTECT FLANGE SURFACES TO PREVENT DAMAGE & SCRATCHING.
7. BREAK & DEBURR ALL SHARP EDGES & CORNERS.
8. CLEAN & PACKAGE IN CLEAR PLASTIC & SEAL PRIOR TO SHIPMENT.

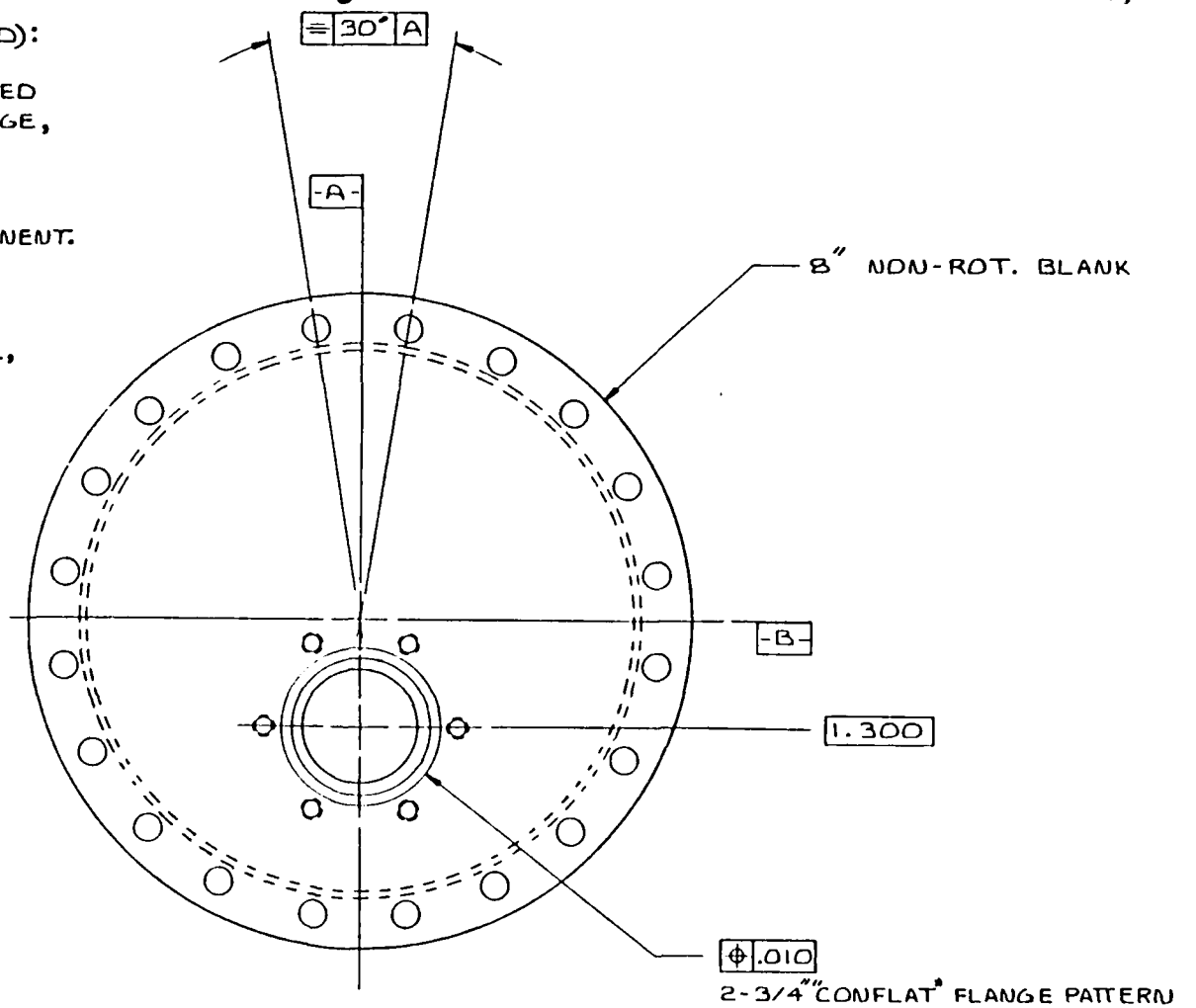

DEACON RESEARCH		
SCALE FULL	APPROVED BY DR8601	DRAWN BY BLM
DATE 3-15-86		REVISED
TO CONFORM TO "CONFLAT" SPECIFICATIONS.		
8"/2-3/4" ADAPTOR FLANGE		DRAWING NUMBER 30-0013

NOTES (UNLESS OTHERWISE SPECIFIED):

1. MATERIAL: BERYLLIUM COPPER, # 25 STRIP, CDA172, .015 THK., 1/2 HARD.
2. FINISH: NO. 63 OR BETTER ("MICROSEAL" 200-1 BY EM CORP. TO BE APPLIED THROUGH DEACON RESEARCH).
3. THIS IS AN ULTRA HIGH VACUUM COMPONENT.
4. USE OF SULFUR BEARING OILS OR ABRASIVES IS PROHIBITED.
5. WHEN PROCESSING (STAMPING, etc.), USE ONLY CIMCOOL, KOOLMIST NO. 77 OR MOBIL CUT-MAX.
6. BREAK & DEBURR ALL SHARP EDGES & CORNERS.
7. BLEND.
8. CLEAN & DEGREASE AND SEAL IN CLEAR PLASTIC BAG PRIOR TO SHIPMENT.

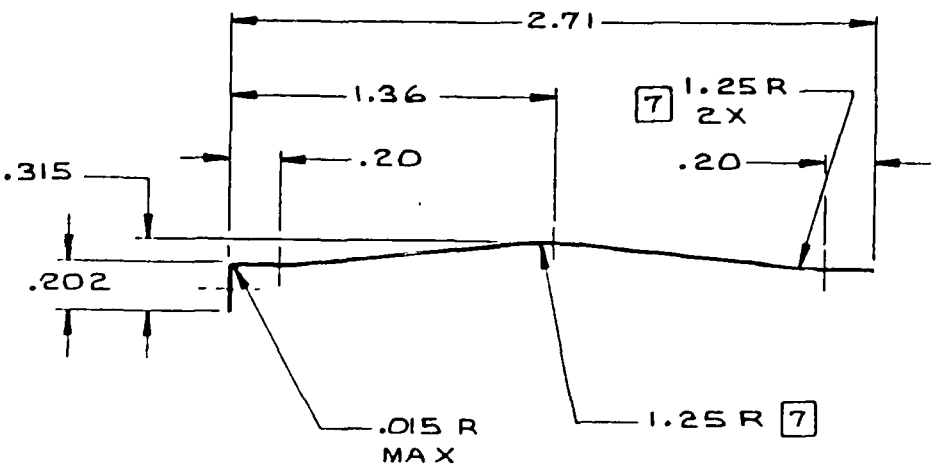

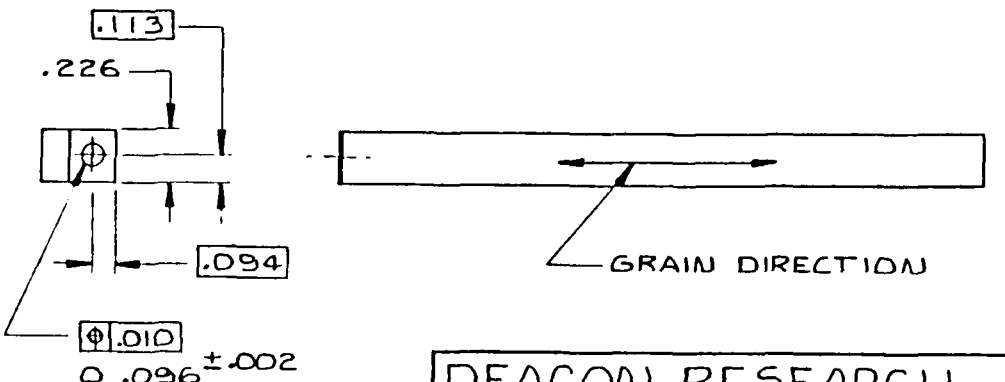

DEACON RESEARCH

SCALE 2/1	APPROVED BY DR8601	DRAWN BY BLM
DATE 3-19-86		REVISED

TOL: .XX ± .01 .XXX ± .005

RETAINER SPRING — DRAWING NUMBER 30-0014

Optical Coating Damage and Performance Requirements in Free Electron Lasers*

David A. G. Deacon
Deacon Research
900 Welch Road, Suite 203, Palo Alto CA 94304

Abstract: The new generation of free electron lasers will place demands on optics which are likely to stress the state of the art in both substrates and coatings. The major problems are to reduce the causes for energy deposition into the optics, and to deal effectively with the resulting thermal effects. In this paper we review the scaling and possible mechanisms of single photon damage, and discuss the thermal phenomena expected in FEL optics.

Presented at the
Lake Tahoe FEL Conference
September, 1985

Free electron lasers are capable of generating high optical power densities in the laser interaction region. This is particularly true for the tapered wiggler which can be designed not to saturate until the intensity at the electron beam reaches hundreds of gigawatts per square centimeter. The optical power density can be reduced by diffraction by the time the laser beam propagates to the nearest optical element. However, the effects on the optics of the intense light beam are likely to be severe, and may become the critical limiting factor on the utilization of FEL technology.

---

* Work supported by Deacon Research internal funds.

It is possible to reduce the intensity at the first optic by placing it far from the interaction region so that free space diffraction causes the laser beam to grow larger, and/or by using a beam expander at grazing incidence. In an oscillator, the resonator mirrors cannot be placed too many Rayleigh ranges away or stabilizing the cavity becomes impossibly difficult. Grazing incidence beam expanders can reduce the intensity by a factor of 20 or so, which is the present limit due to optical figure constraints imposed by the resonator stability condition. In the amplifier configuration, the first optic can in principle be placed far away, but of course the size and cost of the vacuum system increase with the size of the optic. The ability of optics to withstand high intensity radiation without damage is an important limitation on the performance of free electron lasers. In this paper, I summarize the types of damage which are known to occur in high power optics, and discuss the importance to FELs of the relatively new phenomenon of single photon damage.

For damage caused by the laser beam, we can divide the damage mechanisms into two basic categories according to the source of the energy which initiates the chain of events leading to damage. The mechanism can be triggered by an electronic absorption event directly from the photon beam, or indirectly through the absorption of energy into the lattice. Let us call these two classes the direct and the lattice mediated damage mechanisms. In either case, the particular process which

initiates the occurrence of damage may be incapable in itself of significant energy transfer. However, if this trigger process generates sufficient conditions for a phenomenon which does transfer laser energy into the mirror, the trigger process determines the scaling for the damage.

The direct absorption category can be subdivided into single photon and multiple photon absorption events. One might expect the single photon damage mechanisms to be more important in short wavelength lasers where the photon energy becomes appreciable, while the multiple photon mechanisms would tend to be more important in infrared and longer wavelength lasers where the photon energy is small but very high intensities can be produced. Direct absorption effects would include the creation of absorption centers in the optical material, for instance, or any mechanism which is triggered by the photoemission of electrons, such as the cracking of hydrocarbons on the surface of the optic.

The most studied group of mechanisms to date is the lattice mediated category. These can be thermal or nonthermal according to whether the absorbed energy has passed into the lattice on a large scale, or whether phonons are generated. Stress-induced slip or fracture of the surface, fall under this category, as do delamination and other interesting possibilities such as acoustic resonance with phonons coherent with the laser repetition rate.

The formation of a plasma at the mirror surface, which results in cratering [1] would be classified as lattice mediated and thermal since the plasma is apparently initiated [2] by the emission of electrons when the mirror material undergoes slip.

In the following, I will concentrate on the single photon damage mechanism. However, it is useful to begin with a short summary of the effects of thermal damage since both the direct and the lattice mediated mechanisms end up triggering mechanisms which dump heat into the lattice.

Thermal Damage

As is the case for multiple photon damage, thermal damage is characterized by the existence of an intensity threshold below which no effects are apparent in the optic. In the pulsed laser case, one usually describes the threshold in terms of the integrated intensity or the fluence. Thermally absorbed energy produces a distortion of the lattice which builds up internal stress. Damage can be caused by plastic deformation (slip), melting, or fracture. Fracture will occur in bulk optical materials, but in a multilayer structure, it is most likely to occur between layers where the yield stress may be lower than in the bulk material.

Thermal effects typically display a characteristic scaling of the damage threshold fluence F (J/cm^2), which varies as $\tau^{1/2}$ where τ is the pulse length. This dependence arises very simply from the facts that the heat diffusion depth s during the macropulse is proportional to the square root of τ,

$$s \simeq \sqrt{\frac{4\kappa\tau}{\rho C}} \qquad (1)$$

while the total deposited energy ΔE is proportional to τ. The temperature rise T_p during a pulse is then

$$T_p = \frac{\Delta E/V}{\rho C_p} = \frac{A\,F}{\sqrt{4\kappa\rho C_p \tau}} \qquad (2)$$

where κ is the thermal conductivity, ρ is the density, C_p is the heat capacity, $\Delta E/V$ is the energy absorbed per pulse in a unit volume, and A is the absorption coefficient. See Table I for some values for these quantities. For simplicity, we have taken a planar geometry for this and following relations. In a real problem, the geometrical reduction factor must be found by solution of the temporal and spatial boundary value problem.

The temperature rise per pulse is limited by the melting point and the requirement that the thermal stress must remain lower than the yield stresses in the mirror structure. In metals,

the latter requirement limits T_p to the slip temperature [7] which is considerable lower than the melting point. In crystals and glassy materials, the stress is limited by fracture. In multilayer structures, the internal stress may be limited by the delamination stress, depending on how well the layers adhere to each other. For a material with a given damage threshold, the intensity can be increased if τ is reduced. This scaling law fails when the diffusion depth s becomes comparable to the optical absorption depth in the material (the skin depth in metals) where equation (1) breaks down. In the multilayer structures, the yield stress is a function of the depth into the structure, so the τ dependence must be generalized.

A further characteristic of thermal damage is the scaling of the damage threshold with the thermal conductivity κ and the thermal expansion coefficient α. The surface distortion δ is the product of the temperature rise, the depth of the heated volume, and the expansion coefficient. In the pulsed case, the distortion is independent of the thermal conductivity:

$$\delta \simeq T_p \, s \, \alpha = \frac{AF\alpha}{\rho C_p} \qquad \text{(pulsed laser)} \qquad (3)$$

In the high average power case, the distortion depends inversely on the ratio κ/α:

$$\delta = \alpha \, L \, \overline{\Delta T} \simeq \frac{\overline{AI} \, L^2}{(\kappa/\alpha)} \qquad \text{(CW laser)} \qquad (4)$$

where $\overline{I}$ is the mean laser intensity, and L is the thickness of the optic between the heating plane and the assumed "perfect" heat sink.

In the three dimensional geometry typical of an experiment, the geometrical modification to these results must be calculated. However, the surface distortion under the center of the laser beam approaches (3) as the laser mode size w becomes large compared to the thermal diffusion distance ($w >> s$). The distortion under the edge of the laser beam approaches zero under the same conditions. The net angular deflection of the surface will therefore be proportional to $\theta_d \simeq \delta/w$. The (time dependent) optical mode distortion and the thermal stress in the optic are both related to this quantity.

Single Photon Damage

In the early days of the Orsay FEL experiment, my collaborators and I were concerned that the UV light generated in the FEL undulator might damage the oscillator mirrors. At the time, no work had been done at such high fluxes of UV photons, and it was impossible even to guess what might be the level of mirror damage. Of course, we have now observed and reported at least two different degradation processes in the Orsay oscillator mirrors [8], and thanks to the continued efforts of my colleagues at Orsay [9] some detailed information is now available on the character of these processes. These measurements give us a hint of what to expect *from* single photon damage on dielectric coatings, but do not yet allow us to construct a consistent picture of the process.

The direct damage problem has acquired new urgency with the development of plans to construct high power tapered wiggler FEL systems. Since these devices generate harmonics coherently from the laser beam, the energetic photon flux will be orders of magnitude higher than in our prototype system at Orsay. In order to assess the risk posed by single photon damage to the tapered systems, I consider in the following our ability to extrapolate from the Orsay results.

The first thing which is observed as the undulator is

closed onto the electron beam to turn on the FEL interaction is that the losses of the mirrors jump [8,9] by between 4 and 15 × 10^{-4} depending on the coating material. The increased losses have no sharp wavelength dependence, and can therefore be inferred to be uniformly distributed throughout the coating material (at least in the outer layer or so). This process occurs more rapidly than it can be measured. After the undulator light is turned off, these losses slowly and spontaneously disappear [10].

The most likely hypothesis explaining this phenomenon is that the UV photons from the undulator promote electrons from the valence band of the dielectric coating material into localized electron traps in the band gap. The populated traps absorb light in the visible and are continuously replenished by the UV photons. The material dependence of the saturated absorptance level would be explained by differing densities of these localized states. The disappearance of the absorptance in the absence of the UV light would imply that the electron traps in the band gap have a low enough binding energy for thermal depopulation, or that they are sufficiently few in number to be easily bleachable. This hypothesis has yet to be tested experimentally.

At least one additional damage mechanism is observed at Orsay. If the mirrors are exposed to the UV light for a long time, the losses are observed to increase continually [8]. This

increase does not go away when the UV is turned off, and does not disappear when the exposed mirrors are baked in the vacuum. (The losses produced by a third mechanism are improved by an air bakeout [9]). If the undulator is run at K ($=eB\lambda_0/2\pi mc^2$) values below 2, the additional loss levels appear to saturate at a loss level on the order of a few times 10^{-3}.

The spectral dependence of the additional loss contributed by this mechanism has a strong quadratic dependence about the design wavelength of the mirror, which indicates that the absorption is localized at the surface [11]. If the K value is raised to a still higher value (which boosts the intensity of the higher harmonic radiation generated) the losses continue increasing. A measurement of the surface chemical composition via Auger spectroscopy reveals that a surface layer composed of at least 100 A of carbon and silicon is present, while the oxygen originally present in the SiO_2 surface layer is absent.

Surface losses can be caused either by the deposition of an absorbing material (such as carbon) from the vacuum, or by a change in the surface layer which renders it absorbing. In either case, since the intensity of the standing wave varies quadratically with distance near the mirror surface, if the thickness of this layer increases at a constant rate, the optical losses at the center wavelength would increase as the cube of the elapsed time. A measurement of the time dependence of the loss

would be a valuable diagnostic on the layer thickness, and would help to identify the presence of saturation and the causes for it.

The mechanism of the formation of these additional losses is not known. Photoemission from surfaces is known [12] to crack carbonaceous molecules adsorbed on the surface, leaving behind elemental carbon. Photoelectrons can be produced from the valence band of SiO_2 by photon energies above about 15 eV, from the O 2s level with about 22 eV, and from the Si 3s level with about 99 eV photons. Ti impurities (perhaps diffused from the adjacent TiO_2 layer) photoemit from the 4s level with about 34 eV photons. We note that since the dielectric materials we consider are insulators, photoemission charges the surface. In short order, photoemitted electrons are electrostatically reattracted to the surface, in which case they have two opportunities to crack carbonaceous molecules: once on emission, and once on impact!

In synchrotron radiation facilities, a reduction is also seen in the reflection coefficient of uncoated metallic surfaces due to the deposition of carbon. An examination of the mechanism casts light on at least the carbon-related part of the observed dielectric damage. A theoretical model is now available [12] for the carbon deposition process. The model proposes that carbonaceous gases from the residual atmosphere in the vacuum system form a partial monolayer on the optical surface. Incident

photons produce photoelectrons which split the carbon bearing molecules into smaller subunits, sometimes leaving an elemental carbon atom in place on the surface. Many layers of carbon can be built up by this means from a surface layer of adsorbed gas which is at no time thicker than a fraction of a monolayer. The model relates the carbon deposition rate R to the pressure P, the intensity I, and the temperature T.

$$R(P,I,T) = \frac{P\ I}{C_2 P + C_3 T e^{-\Delta E/kT} + I} \qquad (5)$$

where ΔE is the desorption energy. This model has not been fully tested experimentally and the rate constants C_1, C_2, and C_3 are not known, nor is their time or photon energy dependence.

Three limiting cases can be distinguished according to which term in the denominator dominates. If the pressure is very high and the intensity low, a full monolayer of carbonaceous molecules builds up, and each photon has the same probability of adding to the carbon layer. In this limit, the carbon layer growth rate is independent of pressure and linearly dependent on intensity. If the pressure is low and the intensity high, then there will be so many photoelectrons being emitted that the first carbonaceous molecule to be adsorbed will be cracked. In this limit, the growth rate is independent of the intensity and

linearly proportional to the pressure. If the temperature is sufficiently high, the rate is minimized as we see from equation (5), since each carbonaceous molecule spends only a small time adsorbed on the surface. In this limit, the cracking rate is linearly proportional both to the pressure and the intensity.

The carbon layer thus produced would grow at a rate determined by the photoemission and the pressure. The photoemission cross section would be determined at first by the dielectric surface material. One would therefore expect to see a change in the rate of damage after the surface carbon layer grows to a thickness comparable to the penetration depth of the surface photoelectrons or the UV photons. After this time, the rate of carbon growth would be determined by the secondary emission spectrum of the carbon layer itself including whatever impurities it contains.

But photoelectron cracking by itself is not enough to explain the presence of Si and no oxygen in the surface of the damaged Orsay mirrors. Some mechanism is responsible for breaking the Si-O bond and ejecting the O atom. Auger photo desorption [13] with the Si 3s level is not the explanation since it requires photons of too high an energy (99 eV). This mechanism could, however, proceed at Ti impurities.

It is conceivable that some sort of photochemical reaction

takes place at the surface between the Si-O bond and the adsorbed C atom. The production of CO from Si-O and C only requires a few eV of energy. If the mobility of CO is sufficiently high in the carbonaceous surface layer, the CO molecule could diffuse to the surface and escape into the vacuum. We note that this would require a two step process: first a photoelectron cracks a carbonaceous molecule; then a later absorption event results in breaking the Si-O bond. In one limit, the rate equation for such a process would provide a carbon layer growth rate proportional to the square of the harmonic intensity. Since the loss in a thin absorbing layer on a mirror is proportional to the cube of the thickness, this would produce a sixth power dependence of the loss on the fluence. Such a mechanism also requires the penetration of either photons or photoelectrons to the SiO_2 surface, and would eventually turn off as the carbon thickness grows, showing a distinctive saturation behavior.

Unfortunately, there is not enough data at present to confirm these hypotheses. A little experimental work at this stage would go a long way towards sorting out the alternative mechanisms and identifying the scaling behavior of the single photon damage mechanisms.

The rate of increase of the mirror absorption measured at Orsay is about 6×10^{-4} per 100 ma-hr [8] when measured at K = 1.89 and E = 238 MeV. In order to translate this number into something

useful one needs to know the mechanism for the degradation. If the mechanism produces bulk absorption in the coating material, it is possible to derive a cross section for the induced loss. If the damage occurs at the surface, a cross section is inappropriate since the absorption does not depend linearly on the fluence. We consider the situation where the photoelectron cracking of surface carbon is the primary mechanism, in which case, the layer thickness d at a given time will be given by the time integral of the rate (5), integrated over the frequency ω of the damaging photons:

$$d = \int dt \int d\omega \; R(P, I(\omega,t), T(t); \omega, t) \qquad (6)$$

For small layer thickness, the time dependent rate constants in R remain constant (no carbon photoemission saturation), and the absorption from the optical standing wave is proportional to d^3. If we further assume that R is strictly proportional to $P \cdot I$, which is only true in the optimum case of high temperature, we can derive a simple scaling relationship for the induced absorption ΔA:

$$\Delta A = \left(\int d\omega \; P \; D(\omega) \; F(\omega) \right)^3 \qquad (7)$$

where $D(\omega)$ describes the degradation rate, and $F(\omega)$ is the

fluence. The theoretical photon flux density function is readily calculated for the perfect undulator [8]. This dependence has been verified [14] for the Orsay undulator for the first three harmonics. Unfortunately, at this stage, we have very little information on the spectral dependence of the degradation function.

In order to obtain some rough numbers, let us make the drastic simplifying assumption that the degradation function is independent of photon frequency, and that it covers exactly one harmonic of the undulator. We can improve this assumption later as our knowledge grows; making the assumption allows us to attempt quantitative projections for the degradation while at the same time defining the limits of our knowledge. Under this assumption, we can use the theoretical number for the integrated spectral photon flux [8] in the n^{th} harmonic:

$$I_n(\text{photons/cm}^2\text{/sec}) = \frac{N\alpha\bar{I}}{R^2 e}\,\gamma^2 \quad \frac{K^2}{\left(1 + \frac{K^2}{2}\right)^2}\, n \left[JJ\right]^2 \qquad (8)$$

where N is the number of periods in the undulator, α is the fine structure constant, $\bar{I}$ is the average current in the storage ring, R is the distance to the mirror, and [JJ] is a function of K defined in [8]. This integrated expression has the advantage that to first approximation, it is independent of magnetic field

errors.

The Orsay measurement of 6.4×10^{-4} / 100 ma-hr can be transformed into a number for D(n) at the n^{th} harmonic under the above assumption if we know which harmonic (or harmonic region) causes the damage. To obtain a worst-case and a best-case estimate, we calculate two values, one assuming a low harmonic and the other assuming a high harmonic. We obtain

$$\begin{aligned} D(3) &\sim 8.6\times10^{-13}\,cm^2/Torr \quad (3^{rd} \text{ harmonic; } \simeq 7 \text{ eV}) \\ D(15) &\sim 2.2\times10^{-11}\,cm^2/Torr \quad (15^{th} \text{ harmonic; } \simeq 35 \text{ eV}) \end{aligned} \tag{9}$$

The induced absorption can now be estimated from

$$\Delta A \simeq [P\cdot D(n)\cdot F(n)]^3 \tag{10}$$

(subject to the limitations of the above assumptions) once the UV flux generated in the FEL is known. As discussed in the previous section, the maximum tolerable temperature rise in the optics depends on the material used ($\Delta T_{max} \simeq 25\ ^{\circ}C$ in silver [15]). From equation (2) and the laser fluence, we can derive a limiting value on the absorption at which the mirrors damage. Our estimate (9) of the single photon damage coefficient then implies a mirror lifetime, or an upper limit on the harmonic flux.

To take a quantitative example, we look at SiO_2 overcoated Ag mirrors exposed to 50 nsec pulses of 6000 A radiation at a fluence of 1 J/cm^2 per pulse. From (2), the limiting absorptance is $A \leq 4 \times 10^{-2}$. Taking a pressure at the mirrors of 10^{-6} Torr, and assuming it is the third harmonic that is doing the damage, we find from (9) and (10) that the integrated fluence in the third harmonic must be less than $F(3) \leq 4 \times 10^{17}$ $/cm^2$. If the third harmonic flux is generated in the FEL at a photon fluence 10^{-3} of the fundamental, the mirrors will last about 100 pulses until failure. We come to the same conclusion within about an order of magnitude no matter which harmonic might be causing the damage. If the harmonic flux can be attenuated, the mirror lifetime scales up linearly with the attenuation factor. Clearly a high priority must be placed both on reducing the harmonic flux and on obtaining the rate constants and saturation levels for the various single photon damage mechanisms.

It is worth pointing out the assumptions made in arriving at the above result. We assumed that the damage mechanism is carbon deposition as modeled by equation (5); that the other mechanisms are negligible compared to this one; that the scaling with intensity and pressure is linear; and that the rate constants are independent of time. We also assumed that the carbon layer thickness remains thin compared to the optical wavelength; that one harmonic is predominant in the mechanism; and that the rate measured on the Orsay mirrors is valid for the

coated Ag mirrors despite the elemental difference or possible differences in the wavelength or in the fabrication method. It may also be possible to develop countermeasures such as reduction of the carbon during operation.

The first results from the ADONE FEL project are now also available [16]. After 800 ma-hr of exposure at K = 4.8 and E = 600 MeV, induced absorption of 25% was observed in the forward mirror. The loss in the forward mirror remained after prolonged baking in vacuum. Although it is not yet clear what mechanism is at work in this system, their results are at least consistent with the above mechanism. If we go through the same procedure as for the Orsay results, we find values for D(n) close to 10^{-12}. The high K operation of this system produces such copious quantities of harmonics that the D value we derive is almost independent of n.

It is clear that the various dependencies of the degradation process have not been made explicit even within the known model. As we have mentioned, we do not yet know the spectral dependence of $D(\omega)$, which is critically important for any rate calculation. The temperature dependence and material dependence is also largely unknown. Other mechanisms could also play an important role in the degradation. Is the intensity dependence cubic, or sixth power, for instance?

We are beginning a program at Deacon Research to measure some of the scaling characteristics of the single photon damage mechanism. We plan to use a synchrotron radiation facility equiped with a near UV undulator source to expose the sample optics. The UV-induced loss will be measured with the short-pulse cavity ringdown technique [17] inside the vacuum of the sample introduction chamber so that the surface chemistry of the sample can be well controlled. Eventually, we hope to be able to provide a differentially pumped exposure chamber so that the effects of the different carbonaceous gas partial pressures can be determined, and so that countermeasures using oxygen gas or plasma can be attempted.

We expect by this means to supply enough quantitative information to guide the FEL resonator and optics design process. With a knowledge of the mechanism of the single photon damage, it will be possible to calculate by how much the harmonic intensity and pressure at the mirrors must be reduced in a tapered wiggler FEL to make it a viable system. Should adjustments be required in the operation of such a laser to further reduce single photon damage, the scaling information would then be available to direct the modification. In my view, it is preferable to invest now in obtaining this information than to leave the future operation of the FEL precariously dependent on the unknown.

	Thermal Expansion Coefficient $\alpha(/^{\circ}C)$	Thermal Conductivity @25°C $\kappa(W/cm\cdot^{\circ}C)$	Heat Capacity @ 25°C $C_p(J/g\cdot^{\circ}C)$	Density $\rho(g/cm^3)$	Melting Temperature $T_m(^{\circ}C)$
Ge	5.7×10^{-6}	0.67	.32	5.46	937
Cu	1.7×10^{-5}	3.98	.39	8.93	1083
Ag	1.9×10^{-5}	4.27	.24	10.5	962
Au	1.4×10^{-5}	3.15	.13	19.3	1064
SiO_2	$.6\times10^{-6}$	0.014	.75	2.19	1700
SiC	3.5×10^{-6}	0.9	.67	2.96	2700

Table I Some thermal properties of mirror materials [3-6].

References

1. F. Schwirzke, "Unipolar arcing, a basic laser damage mechanism", in Laser induced damage in optical materials, Proceedings of the 1982 Boulder Damage Symposium, NBS Special Publication 669, US Government Printing Office, Washington, 458-478 (1984).

2. H. M. Musal, Jr., "Pulsed Laser Initiation of Surface Plasma on Metal Mirrors", in Laser induced damage in optical materials, Proceedings of the 1980 Boulder Damage Symposium, NBS Special Publication 620, US Government Printing Office, Washington, 227-237 (1981).

3. CRC Handbook of Chemistry and Physics, 54th edition, CRC Press, Cleveland Ohio, (1973).

4. American Institute of Physics Handbook, Third Edition, McGraw-Hill, New York, (1972).

5. CRC Handbook of Material Science, C. T. Lynch, ed., CRC Press, Cleveland Ohio, (1974).

6. Handbook of Thermophysical Properties of Solid Materials, A. Goldsmith, T.E. Waterman, H.J. Hirschhorn, Macmillan, New York (1961).

7. H. M. Musal, Jr., "Thermomechanical stress degradation of metal mirror surfaces under pulsed laser irradiation", in Laser induced damage in optical materials, Proceedings of the 1979 Boulder Damage Symposium, NBS Special Publication 568, US Government Printing Office, Washington, 159-173 (1980).

8. M. Billardon, D.A.G. Deacon, P. Elleaume, J.M. Ortega, K.E. Robinson, C. Bazin, M Bergher, J.M.J. Madey, "Recent results of the ACO storage ring FEL experiment", J. de Physique Colloques C-1, 44, 29-72 (1983).

9. P. Elleaume, M. Velghe, M. Billardon, J.M. Ortega, Appl. Opt. 24, 2762-2770 (1985).

10. J.M. Ortega, private communication.

11. P. Elleaume, PhD dissertation, "Lasers a Electrons Libres sur L'Anneau de Collision dsay", 1984, Universite de Paris Sud, 91405 Orsay, France.

12. K. Boller, R.P. Haelbich, H. Hogrefe, W. Jark, C. Kunz, Nucl. Instr. & Meth. 208, 273-279 (1983).

13. M.L. Knotek, P.J. Feibelman, Phys. Rev. Lett. 40, 964-967 (1978).

14. J.M. Ortega, M. Billardon, G. Jezequel, P. Thiry, Y. Petroff, J. Physique 45, 1883-1888 (1984).

15. H. M. Musal, Jr., "Electron Emission from metal surfaces under pulsed laser irradiation", Proceedings of the international conference on lasers: LASERS '80; Dec. 15-19, 1980, 81-91.

16. M. Ambrosio, G.C. Barbarino, M. Castellano, N. Cavallo, F. Cevenini, M.R. Masullo, P. Patteri, M. Preger, A. Cutolo, "Progress Report on the LELA Project", this conference.

17. D. A. G. Deacon, O. Lee, U.S. Patent Application pending.